Summer 2014

Correlating Molecular Architecture of a Radical Polymer Based Copolymer with its Electrical Transport Properties

Holly Chan
Purdue University

Graduate School ETD Form 9
(Revised 01/14)

PURDUE UNIVERSITY
GRADUATE SCHOOL
Thesis/Dissertation Acceptance

This is to certify that the thesis/dissertation prepared

By Holly Chan

Entitled
Correlating Molecular Architecture of a Radical Polymer Based Copolymer with its Electrical Transport Properties

For the degree of Master of Science in Chemical Engineering

Is approved by the final examining committee:

Bryan Boudouris

Stephen Beaudoin

Rakesh Agrawal

To the best of my knowledge and as understood by the student in the *Thesis/Dissertation Agreement. Publication Delay, and Certification/Disclaimer (Graduate School Form 32)*, this thesis/dissertation adheres to the provisions of Purdue University's "Policy on Integrity in Research" and the use of copyrighted material.

Bryan Boudouris

Approved by Major Professor(s): _____

_____

Approved by: Arvind Varma 07/24/2014

Head of the Department Graduate Program Date

CORRELATING MOLECULAR ARCHITECTURE OF A RADICAL POLYMER BASED COPOLYMER WITH ITS ELECTRICAL TRANSPORT PROPERTIES

A Thesis
Submitted to the Faculty
of
Purdue University
by
Holly Chan

In Partial Fulfillment of the
Requirements for the Degree
of
Master of Science in Chemical Engineering

August 2014
Purdue University
West Lafayette, Indiana

I dedicate this thesis to my mother, Siu Fung Chan.

ACKNOWLEDGEMENTS

I am truly blessed to be given the opportunity to attend graduate school at Purdue University in the School of Chemical Engineering. While this has been a very challenging and intellectually stimulating experience, I could not have completed this thesis without the gracious help and support from my family, friends, and fellow colleagues. The list of all of the individuals that I would to thank formally is innumerous, but to keep this brief, I would like to thank some people in particular.

First, I would like to thank my advisor, Professor Bryan Boudouris for his guidance in my research and for his suggestions in writing this thesis. His availability for providing advice and direction is much appreciated. There are many people that I would like to thank from the POWER Lab group. In particular, thank you Yucheng for running much of the experiments, Liz for your help in polymer synthesis, Aditya for your advice in measuring device mobility, Ryan for your help around the lab, and Rafael for your insight on data interpretation. I would also like to thank Martha and Ned for making lab and my classes, overall, a more enjoyable experience.

I would also like to thank Agnes, Beth, Jennifer, and Ridade for being supportive colleagues and for being such great friends of mine. Their support and companionship have been essential during this program. Finally, I would like to thank my family for their ongoing support during this journey. Thank you, everyone for your loving support and never-ending supply of wisdom.

TABLE OF CONTENTS

Page

LIST OF FIGURES v

ABSTRACT vii

1. INTRODUCTION 1
1.1 Thesis overview 2

2. SYNTHESIS AND CHARCTERIZATION OF CONDUCTIVE POLYMERS 4
2.1 Polymer synthesis techniques 5
2.2 Copolymers 11
2.3 Polymer tacticity 13

3. ELECTRICAL TRANSPORT PROPERTIES OF SEMICONDUCTING POLYMERS AND BASIC ANALYSIS OF THERMOELECTRIC DEVICES 15
3.1 Overview 15
3.2 Thermoelectric device parameters 19
3.3 Two distinct classes of conductive polymers: conjugated polymers and radical polymers 22

4. RESULTS 29
4.1 Overview 29
4.2 Evaluation of the effect of molecular doping of a well-studied conjugated polymer. 30
4.3 Synthesis of poly(2,2,6,6-tetramethylpiperinidyloxyl methacrylate) (PTMA) 33
4.4 Doping PTMA with ethylbenzene sulfonic acid (EBSA) 38
4.5 Synthesis of intramolecular dopants in radical polymers (PTMA-*co*-PVS) 43
4.6 Monomer reactivity of PTMA-*co*-PVS 45
4.7 VS content in PTMA-*co*-PVS as a function of reaction conditions 46
4.8 Functionality of TMPM in PTMA-*co*-PVS (12 mol% PVS) 51
4.9 Hole mobility of PTMA-*co*-PVS (12 mol% PVS) as a function of oxidation time ... 55
4.10 Temperature-dependent hole mobility of PTMA-*co*-PVS (12 mol%) 57

5. FUTURE WORK 59
5.1 RAFT-mediated polymerization of PTMA-*co*-PVS 59
5.2 Blending PTMA with PVS 61
5.3 Determining the electron transport in PTMA-*co*-PVS 63
5.4 Determining the thermoelectric properties of PTMA-*co*-PVS 64

6. CONCLUSIONS 65

REFERENCES 66

LIST OF FIGURES

Figure Page
Figure 1. Depiction of monomer growth to oligomers and polymers..... 5
Figure 2. Characteristics of a controlled polymerization compared with uncontrolled polymerization.. 6
Figure 3. Reaction mechanism in a free radical polymerization 8
Figure 4. Two methods of termination that can take place in a free radical polymerization.. 9
Figure 5. Chain transfer equilibrium in RAFT polymerization. 10
Figure 6. Illustration of different types of macromolecules. 12
Figure 7. Depiction of polymer tacticity 14
Figure 8. Depiction of the bands in a typical conductor, semiconductor, and an insulator.. 16
Figure 9. Depiction of electron transport in a material that exhibits hopping transport.. . 17
Figure 10. Waste heat in the United States as reported by the US DOE in 2008. 20
Figure 11. Schematic representation of a thermoelectric device where charge is conducted due to a thermal gradient..... 22
Figure 12. Molecular structure of PEDOT:PSS..... 24
Figure 13. Reversible redox mechanism of the nitroxide radical 26
Figure 14. Characteristic energy levels of silicon, P3HT, and PTMA. 27
Figure 15. Schematic depicting the measurement of polymer thin film's sheet resistance using a two-point method. 31
Figure 16. The electrical conductivity of blending P3HT with EBSA 32
Figure 17. Reaction scheme by which PTMA was synthesized in a controlled manner using RAFT polymerization. 33
Figure 18. ^{1}H NMR spectrum of PTMPM-RAFT and PTMPM..... 36
Figure 19. ^{13}C NMR spectrum of PTMPM 38
Figure 20. Proposed doping mechanism of EBSA on PTMA based on the stoichiometric ratio of EBSA and PTMA..... 39
Figure 21. Images of PTMA and PTMA-EBSA blended films..... 40
Figure 22. DSC curves of PTMA and EBSA blend.. 42
Figure 23. The electrical conductivity of the EBSA doped PTMA films and the glass transition temperature of the EBSA doped PTMA films..... 43
Figure 24. Modified reaction scheme of the free radical copolymerization of PTMA-*co*-PVS 44
Figure 25. ^{1}H NMR of PTMPM-*co*-PVS) by free radical polymerization 45
Figure 26. Determination of reactivity constants using the Finemann-Ross method. 46
Figure 27. PTMPM-*co*-PVS composition as a function of reaction time..... 47

Figure Page
Figure 28. PTMPM-*co*-PVS composition as a function of monomer composition at a 5 h and 11 h reaction time. 48
Figure 29. Depiction of the proposed synthesis of PTMPM-*co*-PVS at a low concentration(< 50 mol%) and high concentration (>50 mol%) of VS that is initially in the reactor flask 50
Figure 30. FT-IR of PTMA-*co*-PVS (12 mol% PVS) at various lengths of oxidation time. 52
Figure 31. First derivative of the absorption signal in EPR of PTMA-co-PVS (12 mol% PVS) at various lengths of oxidation time. 53
Figure 32. Calibration curve of radical concentration versus total absorption intensity using EPR, the total absorption intensity of PTMA-*co*-PVS (12 mol% PVS) at various lengths of oxidation time, and thecalculated amount of TMPM in the copolymer that exists in the radical state. 54
Figure 33. Voltage versus current density curve of a Al-PTMA-ITO on glass substrate device.. 56
Figure 34. Hole mobility of PTMA-*co*-PVS (12 mol% PVS) at various oxidation times. 57
Figure 35. Temperature-dependent hole mobility of PTMA-*co*-PVS (12 mol% PVS) using space-charge limited devices 58
Figure 36. RAFT-mediated polymerization synthesis route to synthesize PTMA-*co*-PVS. 60
Figure 37. Controlled polymerization of TMPM and VS using a RAFT agent. ^{1}H NMR spectrum of PTMPM-*co*-PVS-RAFT and PTMPM-*co*-PVS 61
Figure 38. ^{1}H NMR spectrum of the VS monomer and PVS polymer 63
Figure 39. Schematic of the device used to measure the Seebeck coefficient of thin films. 64

ABSTRACT

Chan, Holly. M.S.Ch.E., Purdue University, August 2014. Correlating the Molecular Architecture of a Radical Based Copolymer with its Electrical Transport Properties. Major Professor: Dr. Bryan W. Boudouris.

The design and synthesis of electrically-conductive macromolecules can lead to significant improvements in the performance of polymer-based energy conversion devices (*e.g.,* thermoelectric devices). For these organic electronic devices, conjugated polymers have dominated the area of conductive polymers; however, these materials are usually synthesized using conditions that lead to poorly-defined polymers. Furthermore, in these increasingly-standard polymers, the charge transport ability of the polymer thin films is largely affected by the degree of crystallinity, which is a difficult property to control in a reproducible fashion. Therefore, we seek to explore a new class of amorphous, non-conjugated polymers containing a stable radical moiety within the pendant groups (*i.e.,* radical polymers). Among this emerging class of polymers, poly(2,2,6,6-tetramethylpiperinidyloxyl methacrylate) (PTMA) has been used widely in the field of organic radical batteries with high performance metrics being achieved. However, knowledge of the transport properties of PTMA in the solid state is lacking. To this end, we have synthesized PTMA and evaluated the transport properties of this polymer in the pristine and doped state. More specifically, we have incorporated carbon-based dopants with sulfonic functional groups within the polymer chains. Then, we

established how the molecular structure of the copolymer and functionality of the pendant group affect the hole mobility of the copolymer thin film. Through this methodology, we have been able to develop structure-property relationships of the copolymer in order to elucidate how molecular control dictates macroscopic device performance.

1. INTRODUCTION

In 1976, Alan MacDiarmid, Hideki Shirakawa, and Alan Heeger discovered that polymers can be doped to exhibit properties ranging from insulators to conductors.[5–8] Since the advent of their discovery, polymers have made significant strides towards realizing their potential in applications of optoelectronic devices. This is because polymeric materials are capable of exhibiting electrical properties similar to that of metals and inorganic semiconductors while maintaining attractive mechanical properties and processing advantages. Furthermore, polymeric conductors have the added advantage of being earth abundant, which lowers the cost of materials relative to rare-earth metals. Additionally, polymeric materials generally are solution-processable, which enables large-scale processing to occur (*e.g.*, roll-to-roll printing). Another attribute to organic materials is that they are compatible with flexible substrates, which extends the range of applications (*e.g.*, electrically-conductive textiles capable of harvesting energy).[9–11]

However, it is undeniable that there are still many obstacles for organic electronic materials to overcome before they play a substantial role as the active materials of devices in the current energy conversion and energy storage markets. Specifically, in the context of overall costs per net energy produced, organic electronic materials do not perform well.[12–14] This is due to their lower efficiency values when compared with devices fabricated with traditional inorganic materials. Although organic-based materials are not currently as efficient as their inorganic counterparts in electronic applications, the

ability to refine the molecular structure of the organic electronic materials and to optimize the fabrication of macromolecule-based devices provide the opportunity to improve the performance of the polymer-based devices. The primary challenges of common polymer electronic materials are to increase the carrier mobility (*i.e.*, the rate at which the holes in a p-type material and the electrons in an n-type material are transported with respect to an electric field) and the electrical conductivity, which is a function of the carrier mobility and density of carriers in a device. Here, we sought to achieve this through tailored molecular design.

1.1 Thesis overview

The motivation of the research presented here was to control the molecular structure and elucidate the electrical transport properties of an unconventional conductive polymeric material. Particularly, we aimed to elucidate the structure-property relationships of the stable radical polymer, poly(2,2,6,6-tetramethylpiperinidyloxyl methacrylate) (PTMA) while analyzing how charge is transported in a non-conjugated polymeric material. We have quantified the solid-state transport properties of this radical polymer in order to evaluate the efficacy of the material in modules such as thermoelectric devices and solar cells.

Chapter 2 introduces general techniques in polymer synthesis and molecular structure characterization. Chapter 3 details the potential organic electronic applications of the novel material developed here and the theory behind the operation of these devices. In addition, the methods of measuring transport properties are detailed in this chapter. Chapter 4 discusses the synthesis of the radical polymer, PTMA, and the incorporation of

dopants by means of blending and copolymerizing. Then, the microstructure of the copolymer is examined as well as the functionality of the copolymer. Finally, the hole mobility of the copolymer has proven to be improved for the copolymer system relative to the homopolymer system. Chapter 5 discusses the future work of this ongoing project and the future direction that this project has set forth.

2. SYNTHESIS AND CHARCTERIZATION OF CONDUCTIVE POLYMERS

Monomers are small molecules that react to form larger chains of covalently-bonded repeat units. Small chains of repeat units with a molecular weight on the order of 1000 g mol^{-1} or less are nominally-considered oligomers. When the oligomers grow into larger chains, they are considered polymers with molecular weights that easily can exceed 100,000 g mol^{-1} (Figure 1). Polymers can be synthesized by many different synthetic routes that include the general mechanisms of chemically-induced, electrochemically-induced, or photochemically-induced polymerization. Because the formation of polymers is caused by random collisions between reacting species, not all of the polymer chains in the polymer have the same exact number of repeating units. Therefore, polymers have a distribution of molecular weights, which commonly are averaged in two statistical methods to describe the polymer's average molecular weight as the number-average molecular weight (M_n) and the weight-average molecular weight (M_w).[15,16] In one sample of polymers, each polymer chain can be considered as one individual unit. By considering the probability of selecting a polymer chain with a certain number of repeating units, the number-average molecular weight is determined. If instead, each repeating unit is considered one unit, then it is more likely to select a longer chain than a smaller chain. As a result, the chain length is taken into consideration to determine the weight-average molecular weight. These two averages of molecular weight

commonly are used to describe the polymer's molecular weight distribution, which is quantified by the dispersity ($Đ$) according to Equation 2.1.

$$Đ = \frac{M_w}{M_n} \tag{2.1}$$

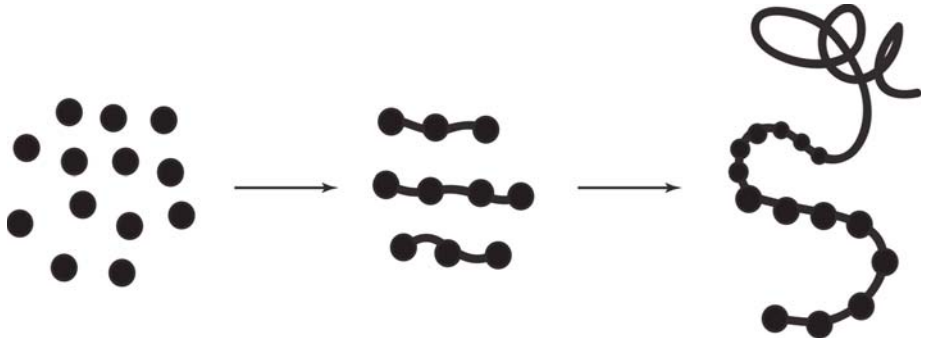

Figure 1. Depiction of monomer molecules (left) forming bonds through a chemical reaction to become oligomers (middle). The oligomers react with additional monomers to become longer chains with many repeat units called polymers (right). Here, the circles indicate monomer molecules, the segments between molecules indicate chemical bonds, the coiled segment indicates the rest of the polymer chain, and the arrows indicate that a reaction has occurred.

2.1 Polymer synthesis techniques

Polymer synthesis can be classified into two categories: 1) a step-growth reaction and 2) a chain-growth reaction. This distinction is determined predominantly by the reacting species. In a step-growth reaction, species of any length may react with one another. In a chain-growth reaction, active species, which may contain an anion, cation, or radical, may only react with a monomer and in this chain-growth polymerization, controlled or uncontrolled polymerization may occur. The classification depends on whether the molecular weight and the molecular weight distribution can be controlled based on the monomer concentration and reaction conditions.

For industrial applications, uncontrolled polymerization techniques are utilized more frequently because they are capable of producing a large quantity of polymer

product and the reaction conditions are less stringent than those used in controlled polymerization techniques. However, controlled polymerization techniques are preferred when certain polymer properties, in which the molecular weight becomes an important handle to control the properties of macromolecular materials, are desired. The distinctive characteristics of a controlled and uncontrolled polymerization are depicted in Figure 2.[15,16] To understand the kinetics of a reaction, it is useful to determine the monomer conversion, which is the concentration of monomer that has reacted divided by the initial monomer concentration. Because uncontrolled termination is suppressed in a controlled polymerization, the number of polymers and the polymer concentration remain constant with conversion. As a result, the degree of polymerization, which is the average number of repeating units in a polymer chain, increases with conversion. In an uncontrolled polymerization, polymer chains terminate sporadically and monomers are initiated throughout the polymerization process. This results in a polymer concentration that increases linearly and a degree of polymerization that is constant with conversion.

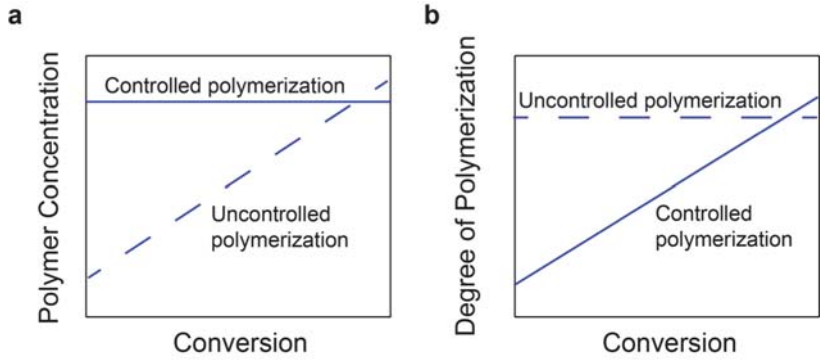

Figure 2. Characteristics of a controlled polymerization compared with uncontrolled polymerization. Conversion is defined as the monomer concentration that has reacted divided by the initial monomer concentration. (a) The polymer concentration is the number of chains per unit volume. (b) The degree of polymerization is the average number of repeat units in a polymer chain.

Because the polymer concentration in a controlled polymerization remains constant throughout the reaction, the molecular weight distribution is narrow. Generally, a dispersity less than 1.3 is regarded as a controlled polymerization. In a controlled polymerization, uncontrolled termination of polymer chains is inhibited until a specified point in time. Uncontrolled termination occurs when a propagating chain reacts with itself or with another propagating chain. At this stage, it is considered an unreactive, or "dead", polymer chain that is not capable of reacting further. If the termination events occur sporadically throughout the polymerization process, the dispersity can increase greatly.[15,16]

An example of this type of termination is found in the common, uncontrolled chain-growth polymerization technique, which is known as the free radical polymerization. Some advantages of this polymerization technique include the compatibility with a wide range of monomers and ability to be performed in an aqueous or organic media. In a typical free radical polymerization, four main reactions occur: initiator decomposition, initiation of monomers, propagation of polymer chains (Figure 3), and termination of polymer chains (Figure 4). First, an initiator and the monomer species are introduced into the reaction vessel. With heat, the initiator decomposes into unstable radical species, which initiate the polymerization of the monomers. When the radical species react with the monomers, the radical transfers to the end of the propagating chain and propagation of the polymer chain begins. Then, the growing chain continues to add repeating units.

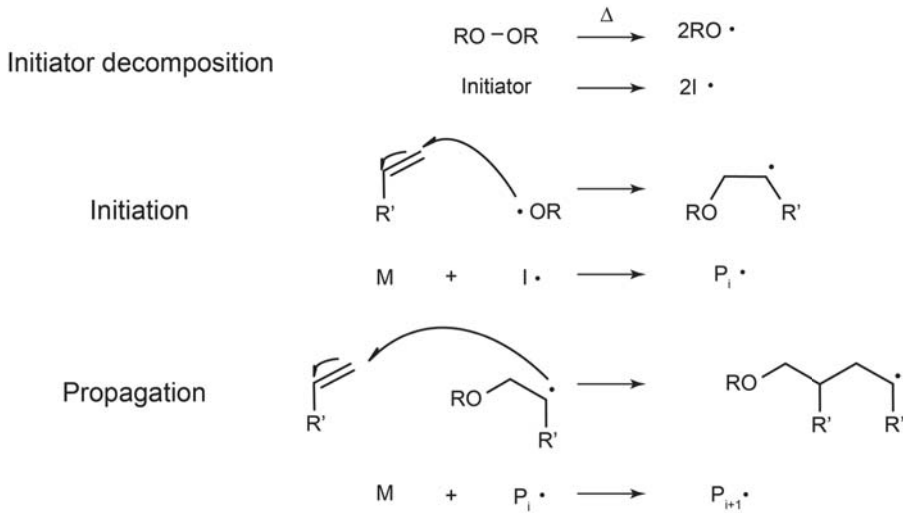

Figure 3. Reaction mechanism in a typical free radical polymerization. The first step involves the initiator decomposition into radical species. Then, the radical species react with monomers, which propagate by reacting with subsequent monomers to form longer chains. Here, R refers to a substituent group, R' refers a different substituent group, I refers to an initiator, M refers to a monomer, and P refers to a propagating chain with i repeat units.

Eventually, the propagating chain terminates by means of disproportionation or combination (Figure 4). Termination by disproportionation occurs when the radical on the propagating chain extracts a hydrogen from another propagating chain. The carbon on the propagating chain that loses the hydrogen forms a double bond with a neighboring carbon. This leads to two unreactive polymer chains. When termination by combination occurs, two radicals each at the end of a propagating chain react to form a bond which creates a single polymer chain with the length that equals to the addition of the two chains that recombined. However, it should be noted that if the repeat units are bulky, combination is not likely due to steric hindrance.

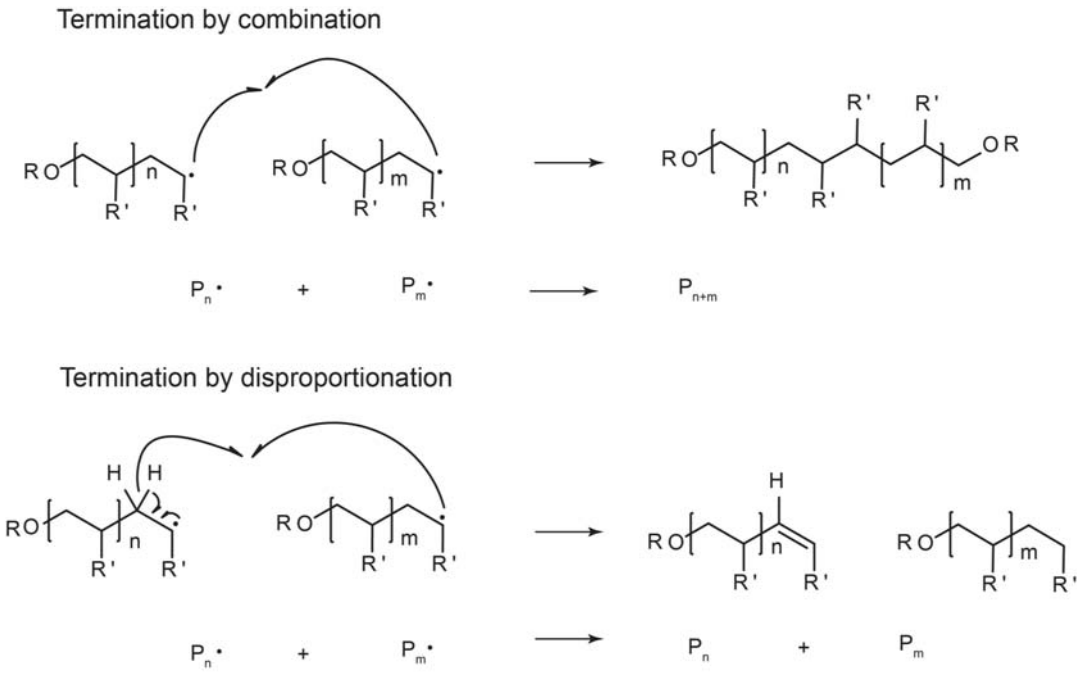

Figure 4. Two methods of termination that can take place in a free radical polymerization. Termination by combination occurs when two propagating chains combine to form one polymer chain with a chain length that equals the sum of the two propagating chain lengths. Termination by disproportionation occurs when one propagating chain extracts a hydrogen from another progagating chain which leads to two unreactive polymer chains. Here, R refers to a substituent group, R' refers a different substituent group, and P refers to a propagating chain with n or m repeat units.

Although polymers can be synthesized more easily with uncontrolled polymerization methods, controlled polymerization techniques offer precise control over the polymer's molecular weight, which enables fine-tuning of the polymer's physical and transport properties. Controlled polymerization conditions can be achieved through ionic polymerization techniques and through controlled radical polymerization methods. Among these radical polymerization techniques, reversible addition-fragmentation chain transfer (RAFT) polymerization has attracted much attention in recent years, because of the relative ease of synthesis.[17] RAFT polymerization employs a reversible chain transfer agent to mediate the reaction. During RAFT polymerization, RAFT agents and initiators are introduced into a reaction flask of monomers. The RAFT agent contains a leaving

group (R) attached to a thiocarbonylthio compound (Figure 5). Here, the Z group attached to the thiocarbonylthio compound dictates the reactivity of the RAFT agent.[4,17] By introducing a RAFT agent, a propagating chain essentially becomes capped with a reactive end group, and this dormant chain is not capable of adding repeating units. In the reaction of an active chain and RAFT agent, a dormant chain (or a polymeric RAFT agent) and a radical species (R·) are produced (right of Figure 5). This polymer unit is now free to add on additional repeating units in an analogous manner, where an active chain can react with a polymeric RAFT agent and transfer the RAFT agent from chain to chain.

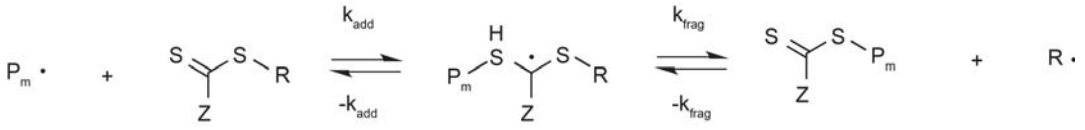

Figure 5. Chain transfer equilibrium in RAFT polymerization.[18] The molecule in the left hand side is known as the RAFT agent, with R representing a leaving group and Z representing a substituent group that dictates the reactivity of the RAFT agent.

While the dormant nature of the polymer chains may be an advantage in some cases (*e.g.*, synthesis of block polymers), it can also pose a problem in the form of undesirable side reactions, which could lead to crosslinking. This is because the thiocarbonylthio group can react with nucleophiles, reducing agents, and oxidizing agents. Crosslinking would lead to chains with higher molecular weights and a larger dispersity. Therefore, after completion of the final polymerization, an additional step is often utilized to remove the reactive terminus. This can be accomplished with several different methods such as the reaction with a nucleophile or the reaction with an excess amount of radical initiator in a protic solvent.[18]

2.2 Copolymers

Macromolecules may contain two or more chemically-distinct repeat units that are covalently-bonded. These macromolecules are known as copolymers. It is possible for copolymers with the same overall composition to exhibit very different macroscopic properties due to differences in the molecular architecture. Therefore, it is important to control the copolymer's microstructure, which can be affected by the synthesis conditions such as the monomer feed ratio, polymerization initiator functionality, sequence of monomer addition, and solvent selection. Schematic representations of various linear copolymer sequences are depicted in Figure 6, where the black and white circles indicate repeating units of different chemical composition.

Copolymers that are considered statistical or random do not have a distinguishable order of repeating units. Alternating copolymers and blocky copolymers have a more ordered structure. Alternating copolymers contain black and white repeat units that appear at every other position. Blocky copolymers contain portions with only black or white repeat units. These copolymers possess properties that are similar to that of blending homopolymers, but without the tendency to phase separate. These sequences can be predicted based on the monomer reactivity ratios in the system.[15,16]

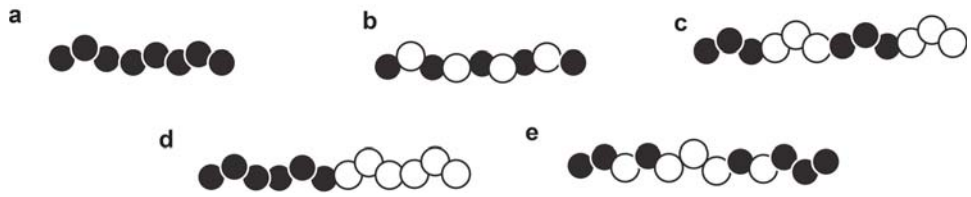

Figure 6. Illustration of different types of macromolecules: a) homopolymer, b) alternating copolymer, c) blocky copolymer, d) block copolymer, and e) random copolymer. Here, the black and white circles indicate repeating units of different chemical composition.

These monomer reactivity ratios quantify the relative reactivity of one monomer type over another monomer type during the polymerization reaction. While there are several models that quantify the reactivity ratios, the terminal model is commonly used because of its overall simplicity. The terminal model assumes that the reactivity is only based on the radical at the end of the propagating polymer and the next monomer to react (Equation 2.2). Here, k_{ij} is the reactivity constant of a propagating chain with end molecule i reacting with monomer j.

$$r_1 = \frac{k_{11}}{k_{12}};\ r_2 = \frac{k_{22}}{k_{21}} \tag{2.2}$$

Using this model, Mayo and Lewis developed the relationship of polymer composition as a function of reactivity ratios and instantaneous monomer composition. At low conversion, the reactivity ratio can be approximated using the Finemann-Ross linear method (Equation 2.3 and 2.4). Here, m_i refers to the polymer composition of repeating unit i and M_i refers to the instantaneous monomer composition of repeating unit i.[19,20]

$$\frac{F}{f}(f-1) = r_1\frac{F^2}{f} - r_2 \tag{2.3}$$

$$f = \frac{m_1}{m_2};\ F = \frac{M_1}{M_2} \tag{2.4}$$

At low conversion (~10%), the instantaneous monomer composition is approximated as the initial monomer composition. Using this method, the molecular sequence of the copolymer can be determined. While the reactivity ratios aid in giving a visualization of the copolymer architecture in a 2D manner, the tacticity furthers this by providing an image of the copolymer in a 3D manner.

2.3 Polymer tacticity

Therefore, to elucidate the chemical microstructure of the polymer spatially, the tacticity of the polymer can be determined. Tacticity refers to the orientation of the pendant groups along the polymer chain. This molecular property, at least in part, dictates the packing of polymer chains. This packing impacts the polymer crystallinity, which affects its electrical transport capability, and also the polymer density, which affects its tensile strength. ^{13}C NMR spectroscopy can be used to examine the tacticity of the polymer.[21–23] The pendant groups can be oriented on the top or bottom of the polymer backbone. Because of the different molecular configurations, the electron environment can vary for each carbon. This causes the chemical shifts to move slightly depending on the shielding. This information can be used to quantify the tacticity. For an isotactic polymer (mm), all the pendant groups are arranged spatially on the same side of the polymer chain (*e.g.*, out of the page, as shown in Figure 7). For a syndiotactic polymer (rr), the pendant groups are arranged on alternating sides of the polymer chain. When the distribution of pendant groups are random along the polymer chain, the polymer is considered atactic (rm).[15,16]

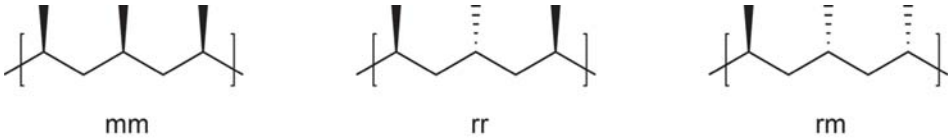

Figure 7. Depiction of tacticity, where mm depicts an isotactic structure, rr depicts a syndiotactic structure, and rm depicts an atactic structure. The solid wedge corresponds a pendant group that is coming out of the plane of the page and the dotted wedge corresponds to a pendant group that is going into the plane.[15,16]

Ultimately, with an understanding of the molecular microstructure of the copolymer chemically and spatially-specific polymer properties can be enhanced in a manner that enables the polymer to increase in functionality. In this work, we utilized the molecular structure to correlate with the electrical transport properties of the copolymer system, and the results will be addressed in the following chapters.

3. ELECTRICAL TRANSPORT PROPERTIES OF SEMICONDUCTING POLYMERS AND BASIC ANALYSIS OF THERMOELECTRIC DEVICES

3.1 Overview

Materials can be divided into three main categories (*i.e.*, metals, semiconductors, or insulators) to describe their electrical properties. The various classifications are characterized by the magnitude of the electronic band gap of each set of materials (Figure 8). These bands, on either side of the band gap, are formed by closely-spaced electron orbitals that are near one another in energy. The band gap (E_g) is the difference between the conduction band, or the lowest unoccupied band, and the valence band, or the highest occupied band. For semiconductors and insulators, band transport is used to describe current flow (*i.e.*, the net flow of charge). The band structures of semiconductors and insulators are similar, except insulators have a larger band gap (*e.g.*, $E_g \geq 5$ eV).[24] Because of the larger band gap in insulators, few electrons are promoted from the valence band to the conduction band. Thus, current flow is very small for insulators.

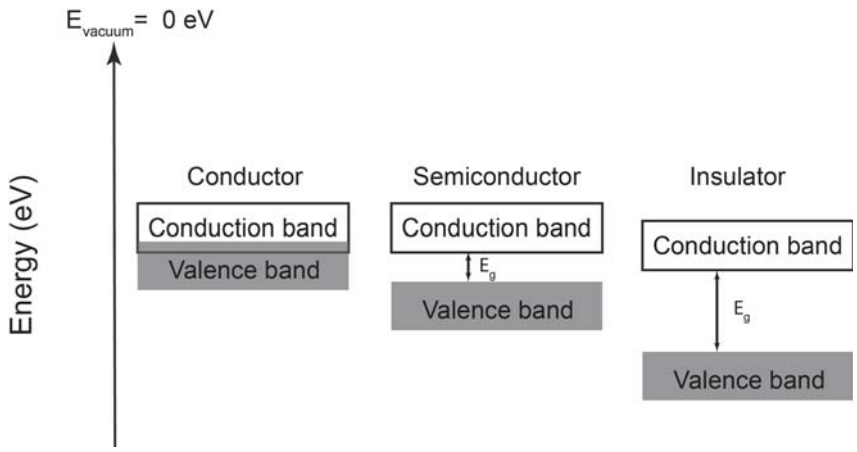

Figure 8. Depiction of the bands in a typical conductor, semiconductor, and an insulator. In a conductor the conduction band overlaps with the valence band. The energy band gap (E_g), which is the difference between the conduction band and valence band, is larger for the insulator than the semiconductor.

On the other hand, the "electron sea" model generally is used to describe the conduction in metals.[25] Metals are composed of atomic cores that are held together by the valence electrons, which are shared among the atoms. Because of the free nature of these electrons, metals are excellent conductors. For metals, the bands overlap, such that there is no gap between bands. Instead, they are characterized by their work function.

Although organic materials cannot compete with metals in terms of possessing high electrical conductivity, organic materials exhibit electrical properties comparable to inorganic semiconductors. Some organic materials, which have relatively high degrees of crystallinity, exhibit band-like transport.[26] However, most organic materials behave in a similar manner to inorganic semiconductors or inorganic insulators where the electrons are localized by defects and the carriers encounter multiple trapped sites.[27,28] This conduction mechanism is known as hopping transport (Figure 9). When an electric field is applied, electrons travel along the transport level. However, these electrons may collide with one another, causing them to lose energy and fall into shallow traps, which are less

of an energy difference from the transport level than the available thermal energy. Therefore, it can gain enough energy (*e.g.*, through molecular vibrations) to be promoted back to the transport level. In a similar manner, the electrons may fall into deep traps, which are generally much larger in energy difference than the available thermal energy. These electrons are unable to overcome the deep traps without an additional energy boost, which comes at a much longer frequency than that associated with thermally-activated energies like those at shallow traps.[29]

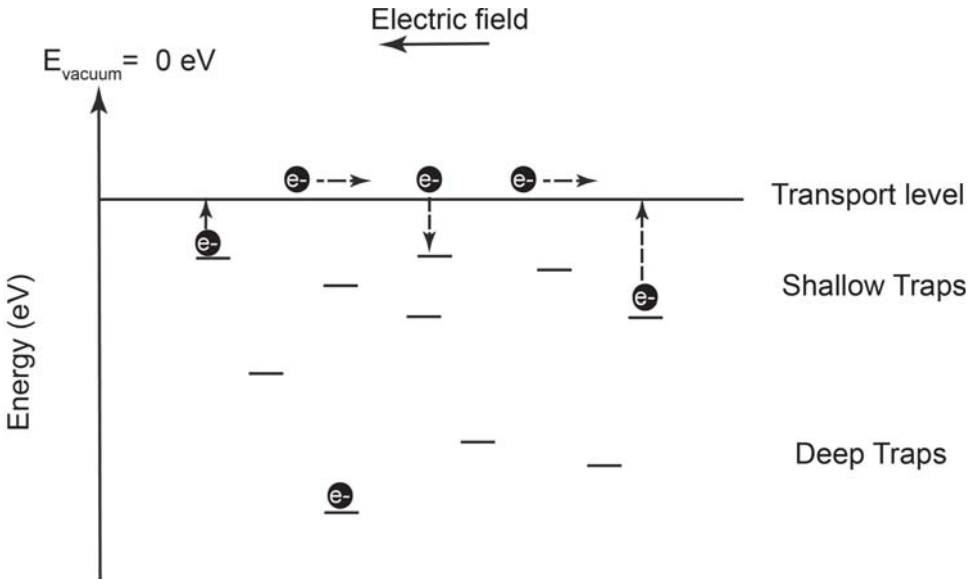

Figure 9. Depiction of electron transport in a material that exhibits hopping transport. With an applied electric field, electrons travel within the material at the transport level. Some electrons fall into the shallow traps. Because these shallow traps are <kT (where k is the Boltzman constant and T is the temperature) in energy from the transport level, the electrons are able to overcome it with enough thermal energy. However, deeper traps are >kT, such that the electrons are unable to get out of the trapped state without an external energy source.

The speed at which the electrons transport through the material can be used to aid in the hypothesis of whether the material is exhibiting band-like transport or hopping transport because this would indicate the degree of traps within the semiconductor.[30] The speed at which charge carriers travel within a material in the presence of an electric field

is known as the carrier mobility. From the equipartition of energy theorem, under thermal equilibrium, the average kinetic energy of an electron is a function of the Boltzman constant (k) and temperature (T) (Equation 3.1). Here m_e^* is the electron effective mass, m_h^* is the hole effective mass, and v_{th} is the average thermal velocity.[30]

$$\frac{1}{2}m_e^* v_{th}^2 = \frac{3}{2}kT \tag{3.1}$$

When an electric field (E) is applied, the electrons experience a force that causes the electrons to drift. By performing a momentum balance of the momentum gained by the electron due to the electric field and the momentum lost during collisions, the carrier mobility can be determined (Equation 3.2 and Equation 3.3). Here, q is an electron charge, τ is the mean free time between collisions, v_d is the drift velocity, μ_e is the electron mobility, μ_h is the hole mobility.[30]

$$-qE\tau = m_e^* v_d \tag{3.2}$$

$$\mu_e = \frac{v_d}{E} = \frac{q\tau}{m_e^*};\ \mu_h = \frac{v_d}{E} = \frac{q\tau}{m_h^*} \tag{3.3}$$

At mobility values < 1 $cm^2\ V^{-1}\ s^{-1}$, materials generally are considered to conduct charge through hopping transport.[30,31] At higher values, materials are governed by band-like transport. Intuitively, from Equation 3.3, carrier mobility is affected largely by the mean free time between collisions, which in turn, is affected by scattering predominantly through lattice vibrations and phonons.[32] In organic materials that are governed by band-like transport, there are a limited amount of energy traps.[33] This means that the electrons do not require additional energy to maintain their locations at the transport level. An increase in temperature works counterproductively for these materials, because an

increase in temperature increases the amount of phonons (*i.e.*, through lattice vibrations). These occurrences lead to scattering and lowering of the mean free time between collisions. As a result, carrier mobility decreases with increasing temperature. On the other hand, for organic materials that are governed by hopping transport, an increase in temperature allows the carriers to have more energy, which allows some carriers to overcome the trap states through thermally-activated processes. Therefore, carrier mobility increases with increasing temperature when the material is governed by hopping transport.[27,28]

Understanding the conduction mechanism and transport properties of the material is key to developing robust material that would perform well in electronic applications. Furthermore, with this knowledge, it is possible to obtain an understanding of the material at a molecular level in order to tailor systematically the molecular structure of a material to improve its transport properties and functionality.

3.2 Thermoelectric device parameters

In recent years, conductive macromolecules have been utilized in existing and emerging technologies (*e.g.*, memory devices, biosensors, thermoelectric devices, rechargeable batteries, fuel cells, and photovoltaic cells).[9,10,34,35] In particular, conductive macromolecules have the potential to make significant progress in the field of thermoelectric devices, which convert heat directly into electricity.[36,37] In the United States about 60% of the energy produced in the United States is wasted as dissipated heat.[37] In 2008, the US Department of Energy estimated that about 1,500 TBtu yr^{-1} of energy is dissipated in the form of heat, which is equivalent to more than 1.8 billion

barrels of oil.[38] Furthermore, the majority of waste heat is produced at a low temperature scale (*i.e.*, $T < 230$ °C) through water steam boilers on an industrial and a commercial setting (Figure 10). In this relatively low temperature regime, organic materials are capable of playing a significant role in heat-to-electricity conversion applications.

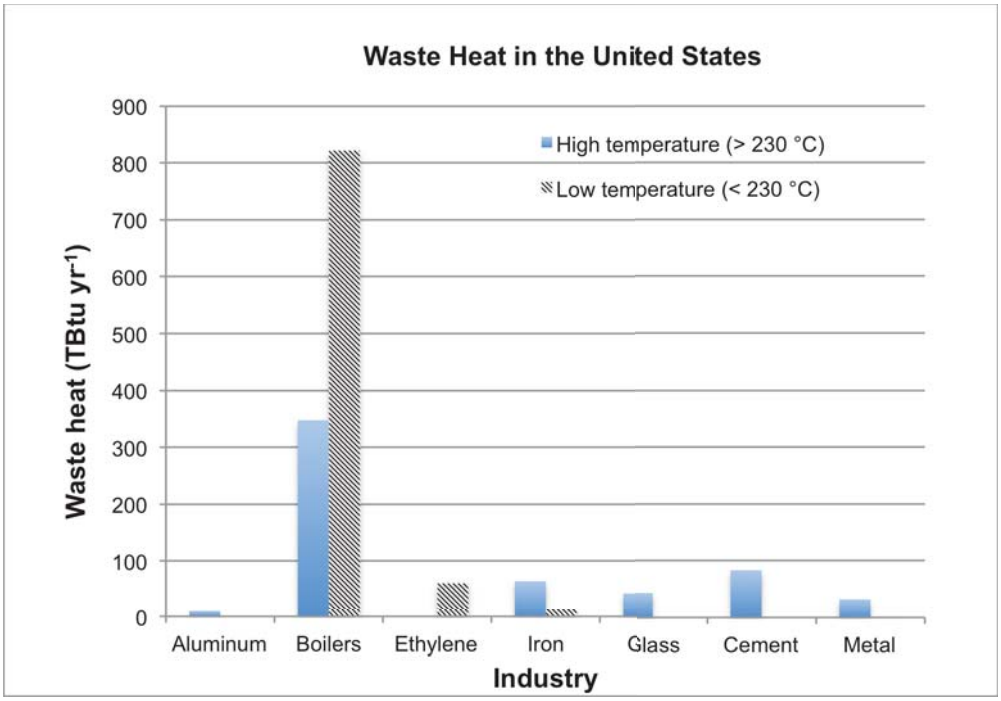

Figure 10. Waste heat in the United States as reported by the US DOE in 2008. The amount of waste heat is listed by industry and categorized by the temperature of the exhaust heat.[38]

In order to obtain a high-performance thermoelectric device, it is necessary to understand the transport phenomena at the nanoscale and in the bulk. A thermoelectric module contains pairs of n-type and p-type legs that are connected thermally in parallel and electrically in series (Figure 11).[39–41] Each of these legs is characterized by the figure of merit, zT.

$$zT = \frac{\sigma S^2 T}{\kappa} \tag{3.4}$$

$$\sigma = e(n\mu_e + p\mu_h) \tag{3.5}$$

Here, S is the thermopower (or Seebeck coefficient), σ is the electrical conductivity, e is the fundamental charge, n is the number of electrons, μ_e is the electron mobility, p is the number of holes, and μ_h is the hole mobility, σS^2 is the power factor, T is the average absolute temperature of the system and $\varkappa$ is the thermal conductivity.[39] From the figure of merit, it is apparent that an ideal material will have low thermal conductivity to maintain a large temperature gradient and a high power factor. Intrinsically, organic materials have a low thermal conductivity, which is several orders of magnitude lower than inorganic materials.[42] The lowest bound to the thermal conductivity commonly is known as the amorphous limit.[43,44] In inorganic materials, the lattice structure facilitates the movement of phonons. Therefore, point defects by alloying and low-dimensional structures (*e.g.*, quantum dots and nanowires) by nanostructuring frequently are introduced into inorganic materials to scatter phonons.[45,46] Because organic materials contain an amorphous regime, if not an entirely amorphous phase, these materials possess close to the lowest theoretical limit of thermal conductivity.

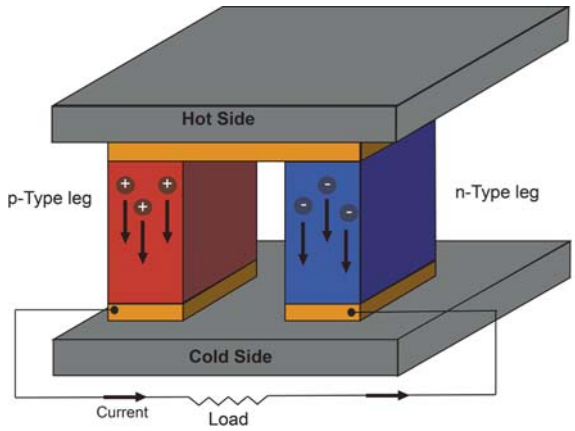

Figure 11. Schematic representation of a thermoelectric device where charge is conducted due to a thermal gradient. The p-type, hole-conducting leg is shown in red and the n-type, electron-conducting leg is shown in blue.

While the primary challenge in inorganic materials is to reduce the thermal conductivity, in organic materials, the challenge is to increase the electrical conductivity which currently can range between 10^{-8} S cm^{-1} and 10^{4} S cm^{-1}.[36] The current preferred method to increase the electrical conductivity of organic material is to employ doping strategies.[47–49] Even though the transport theory and doping mechanisms of organic materials are not well-understood, the transport properties of commonly studied conjugated polymers have improved significantly over the years.[36]

3.3 Two distinct classes of conductive polymers: conjugated polymers and radical polymers

In the backbone of conjugated polymers, carbon-carbon bonds alternate between single and double bonds. Because each carbon atom in the backbone is covalently-bound to three other atoms, sp^2-hybridization takes place. This hybridization causes the electrons in the p-orbital to overlap and form a π-bond, allowing this type of polymer to be referred as a π-conjugated polymer. The delocalization provides a "highway" for

charge transport, which is facilitated with ordered or crystalline domains.[50] Because of the ability of carriers to traverse within the material, the material is capable of conducting charge to the extent that enables it to function as the active layer in thermoelectric devices.[36,51] Among π-conjugated materials, iodine-doped polyacetylenes exhibit the highest power factor of 2000 μW m^{-1} K^{-2} (with $\sigma \sim 50{,}000$ S cm^{-1} and $S \sim 20$ μV K^{-1}) at 300 K, which approaches the value of the best thermoelectric materials.[36] However, halogen doped polymers are unstable due to the volatile nature of the dopants. Therefore, a wide variety of more stable organic thermoelectric materials have been investigated and a comparison of the thermoelectric properties of commonly-studied π-conjugated materials and inorganic materials is shown in Table 1.[36,40,52-56]

Table 1. Thermoelectric properties of common p-type inorganic and organic materials. Here, S is the thermopower (or Seebeck coefficient), σ is the electrical conductivity, σS^2 is the power factor, T is the average absolute temperature of the system, and $\varkappa$ is the thermal conductivity.

Material	Description	σ (S cm^{-1})	S (μV K^{-1})	$S^2\sigma$ (μW m^{-1} K^{-2})	$\varkappa$ (w m^{-1} K^{-1})	z (K^{-1})	Ref.
Cu		5.8×10^5	1.83	190	398	4.8×10^{-7}	40
Si		290	450	5.8×10^3	145	4.0×10^{-5}	40
Bi_2Te_3		600	140	3.5×10^3	1.32	2.7×10^{-3}	52
Te	Nanowires	0.08	408	1.3	2	7.0×10^{-7}	53
Polyacetylene		6.4×10^3	20.6	270			54
Polyacetylene	Doped with iodine	5.0×10^4	20	2×10^3			36
Polypyrrole		200	7	0.045			36
PEDOT:PSS		1.3	18.9	0.05	0.24	2.0×10^{-7}	53
PEDOT:PSS	Coated around Te nanowires	19	163	51	0.22	2.0×10^{-4}	53
PEDOT:PSS	Post-treatment with DMSO	950	65	400	0.26	1.2×10^{-3}	55
PEDOT:Tos		300	40	38	0.37	8.4×10^{-4}	56

As expected, traditional inorganic semiconductor materials (*e.g.*, Bi_2Te_3) possess superior electrical properties compared with pristine conjugated materials.[52] However, over the past few years, one notable conjugated polymer, namely poly(3,4-ethylene

dioxythiophene) (PEDOT), has made large breakthroughs with improvements in electrical transport properties, whereby doubling its thermoelectric figure of merit.[56,57] The properties of PEDOT are improved significantly when it is p-type doped with the negatively-charged counterions, such as poly(4-styrenesulfonic acid) (PSS) (Figure 12).[51]

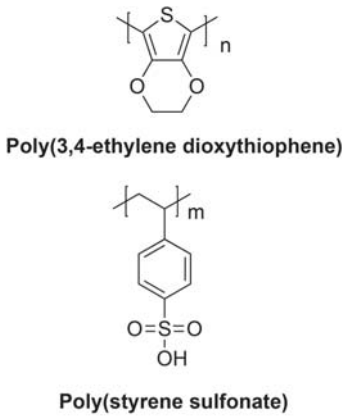

Figure 12. Structure of PEDOT (above) and PSS (below). PSS is used as the counterion to p-type dope PEDOT and form PEDOT:PSS.

In 2011, researchers have demonstrated that an all-organic system achieved a zT = 0.25 at room temperature.[56] In this system, PEDOT was synthesized in the presence of tosylate, a small molecule form of PSS.[56] Furthermore, in 2013, by immersing fabricated PEDOT:PSS films in a heated ethylene glycol bath, the excess PSS was removed, and a record high zT = 0.42 at room temperature was reported.[55] Considering that PEDOT is hydrophobic and PSS is hydrophilic, it is likely that in these PEDOT:PSS films, strands of PSS agglomerate together as opposed to PSS polymer strands uniformly surrounding and doping PEDOT polymer strands. By removing the excessive, electrically-insulating PSS clusters, the transport properties of the system were improved. The record high result highlights the importance of optimizing the doping level and the polymer thin film

microstructure by means of a solvent post-treatment. Moreover, these results show that in just a few years, the transport properties of a polymeric system can improve significantly.

Although π-conjugated polymers have emerged in a variety of organic electronic applications (*e.g.*, solar cells and memory devices)[35,49], the majority of the syntheses, besides the Grignard metathesis (GRIM) method, lead to poorly-controlled molecular weights and molecular weight distributions.[58,59] Furthermore, many of the synthetic polymerization protocols used require metal catalysts.[60] For instance, Suzuki coupling is frequently used to synthesize polythiophenes with a palladium catalyst.[61] The metal impurities are difficult to remove from the polymer. This impacts electronic devices negatively in several ways by: reducing the lifetime of electronic devices, causing film defects, and producing trap sites in the band gap.[62,63]

In this regard, an emerging class of polymers has its advantages. Specifically, radical polymers can be synthesized using facile metal-free methods, such as through the free radical polymerization mechanism.[64] Radical polymers contain a non-conjugated backbone with radical-bearing pendant groups, which are stabilized by bulky neighboring substituent groups. While π-conjugated polymers transport carriers at the polymer backbone, radical polymers transport carriers at the side pendant groups. At the stable radical sites, the hopping charge transport occurs through a reversible oxidation-reduction (redox) mechanism, as shown in Figure 13.[65] The nitroxide radical may undergo oxidation to form the oxoammonium cation (hole-transporting or p-type transport). Likewise, the nitroxide radical may reduce to form the aminoxy anion (electron-transporting or n-type transport).[34,66] This reversible one-electron reaction can be induced

in the presence of an electrolyte, which is applicable in organic radical batteries, or in the presence of an electric field as is the case for solid-state transport.[4,34]

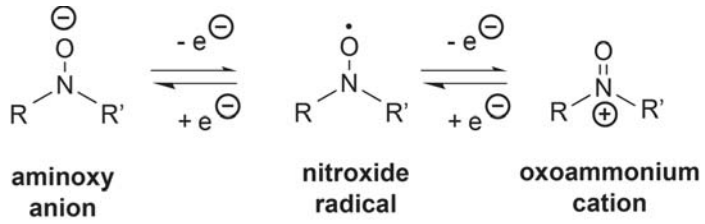

Figure 13. Reversible redox mechanism of the nitroxide radical. The aminoxy anion gains an electron to become a nitroxide radical, which in turn can gain another electron to become an oxoammonium cation. R represents a substituent group and R' represents a different substituent group.[2,65]

Among radical polymers, poly(2,2,6,6-tetramethylpiperidinyloxy methacrylate) (PTMA) is well-studied because of its high electrical capacity, thermal stability at high temperatures, and ability to be stored for over a year without degrading.[34,66,67] Since being discovered by Nakahara in 2002, PTMA has been studied extensively in organic radical battery applications. In addition, an all-radical polymer memory device, which contained PTMA, has been successfully fabricated with an on-off ratio of four orders of magnitude. The retention cycles of the on and off states were repeatable for over 10,000 times. Furthermore, the states were repeatable after a month.[68] This indicates that PTMA has potential to be used in the solid state for electrical applications.

The molecular structure of PTMA recently has been studied by means of molecular simulations using density functional theory (DFT) calculations.[69] In their work, the researchers determined that the carbons along the PTMA backbone are about 12 Å apart while the carbons along a similar polymer, poly(methyl methacrylate), contains carbons that are roughly 2-3 Å apart in the backbone. This is attributed to the fact that PTMA has larger substituents groups, which force the carbons apart. Furthermore, in

their work, they estimated that electron transfer occurs about 84% between polymer chains and 16% within the same chain. Because electron transport predominantly occurs intermolecularly, decreasing the distance between chains can impact charge transport significantly. This idea has been implemented by introducing dopants to fill the void space, such as with the introduction of 4-hydroxy-2,2,6,6-tetramethyl-piperidinyl-oxidanyl (TEMPO-OH) molecules, the radical-bearing small molecule analog of PTMA, which increased the conductivity of PTMA.[4]

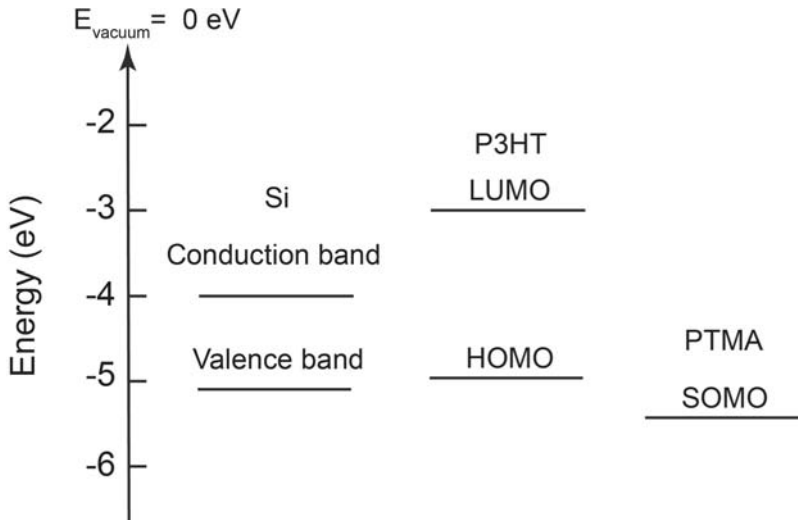

Figure 14. Characteristic energy levels of silicon, a common conjugated polymer, poly(3-hexylthiophene) (P3HT), and PTMA. LUMO stands for the lowest unoccupied molecular orbital, HOMO is the highest occupied molecular orbital and SOMO is the singly occupied molecular orbital.

However, charge transport in radical polymers is still not well-understood. Yet, radical polymers are similar to conjugated polymers in some ways. For instance, the transport energy level of PTMA is analogous to that of conjugated polymers. In conjugated polymers, the LUMO level is the lowest unoccupied molecular orbital, which is similar to the conduction band for inorganic materials. The HOMO level is the highest occupied molecular orbital, which is analogous to the valence band for inorganic

materials. The difference between these two levels is the band gap. In radical polymers, the SOMO level, or the singly occupied molecular orbital, is the energy at which the lone electron resides. These energy levels are characteristic of the material and are important in dictating the material's functionality in a power conversion device. In this work, we will use intramolecular dopants to elucidate the effect of dopants on the molecular structure and transport properties of PTMA with the aim being to improve the solid-state electronic transport properties of this emerging class of electronically-active polymer.

4. RESULTS

4.1 Overview

Our main focus in this work was to elucidate the structure-property relationships of a novel, emerging class of conducting polymers (*i.e.*, radical polymers) and to enhance the electrical properties of the radical polymer system. Currently, the amount of information on radical polymers in electrically-oriented applications is minimal compared to the wealth of information on conjugated polymers. Even though these two different classes of conducting polymers differ in the driving force behind the charge transport, the basic scheme behind the charge transport mechanism is somewhat similar. Therefore, before improving the transport properties of the less well-studied radical polymer system, in our own laboratory, we established how doping was accomplished in a well-understood conjugated polymer system.

For instance, small molecules with sulfonic functional groups have been known to possess ionic conductivity values $\sim 10^{-2}$ S cm^{-1} under dry conditions.[70] Therefore, dopants with sulfonic functional groups have the potential to significantly improve the transport properties of a polymer system. As such, we examined the effects of incorporating the organic dopant, ethylbenzene sulfonic acid (EBSA), to a commonly-researched conjugated polymer, poly(3-hexylthiophene) (P3HT). This served as a base-line case, as this system has been studied previously.[71] In particular, we report the electrical conductivity of P3HT as a function of EBSA loading. After determining that EBSA is

capable of significantly improving the transport properties of a conjugated polymer, we examined if EBSA had the potential to be used as a dopant in a radical polymer system.

4.2 Evaluation of the effect of molecular doping of a well-studied conjugated polymer

In these experiments, the electrical conductivity (σ) was measured for the polymer thin films in a two-point method, as shown in Figure 15. First, glass substrates were sonicated for 10 m in a beaker of acetone, followed by chloroform, and then isopropanol. Films were fabricated by spin-coating or drop-casting the polymer onto the substrates from solution, annealing the dry film at a prescribed temperature, and thermally-evaporating metal as top contacts. Using a Lakeshore cryogenic probe station equipped with a Keithley 2400 source meter, probe tips were placed on top of the metal contacts. A voltage (V) was applied between the contacts and the current (I) was collected to generate an I-V plot. The inverse of the slope of this line can be used to calculate the sheet resistance (R_S). The electrical conductivity, which is the inverse of electrical resistivity, was calculated using Equation 4.2. Here, A is the channel contact area, L is the channel length, and ϱ is the electrical resistivity.

$$\rho = \frac{R_S A}{L};\ R_S = \frac{V}{I} \tag{4.2}$$

After measuring the thickness of the film using a profilometer and the electrode dimensions using an optical microscope equipped with ImageNow software, the conductivity was calculated readily.

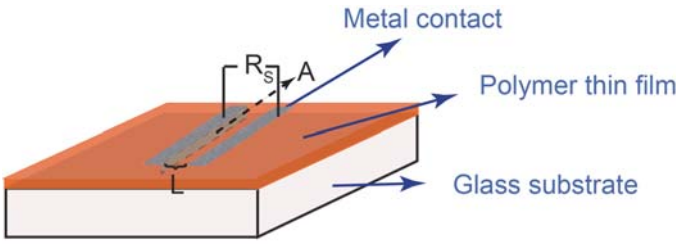

Figure 15. Schematic depicting the measurement of polymer thin film's sheet resistance (*R*) using a two-point method.

It is well-established in the literature that molecular dopants can impact the conductivity of π-conjugated polymers.[36,48,55] For instance, sulfonic acid derivatives have been used extensively to produce self-doped polymers containing polyaniline, polythiophene, and polypyrrole.[72] In one specific system, 4-ethylenebenzene sulfonic acid (EBSA) was used as a counterion dopant for poly(3-hexylthiophene) (P3HT).[71] At 1 wt% of EBSA, the hole mobility increased almost two orders of magnitude to a maximum hole mobility value of 0.11 $cm^2 V^{-1} s^{-1}$.[71]

A similar procedure was conducted here to study the molecular doping of P3HT and its impact on the conductivity. Specifically, P3HT was dissolved in chlorobenzene. EBSA was introduced as a dopant into this solution, and the combined solution was stirred at 60 °C overnight. Films were made by drop-casting the solution onto glass substrates, and, then, the devices were annealed for 20 m at 120 °C. Subsequently, metal contacts were thermally-evaporated onto the films, and the electrical conductivity was measured for the resulting films (Figure 16).

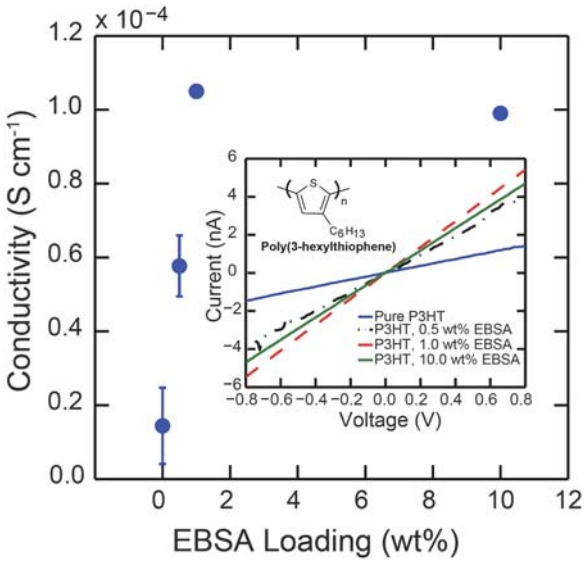

Figure 16. P3HT was dissolved in chlorobenzene with EBSA as the dopant. The solution was drop-casted and the electrical conductivity was calculated as a function of EBSA loading. The inset shows the raw data of current-voltage sweeps of the EBSA doped P3HT films. The chemical structure of P3HT is shown as well.

At a doping level of 1 wt% EBSA, the electrical conductivity increased by an order of magnitude (Figure 16). This result indicates that a small amount of EBSA has the potential to increase the conductivity of a polymer significantly. However, this optimum amount of dopant at such a low concentration varies from system to system. For instance, the conductivity of PEDOT increased by 6 orders of magnitude at 20 mol% of tosylate.[56] In the P3HT-EBSA system, at a higher loading of EBSA, the conductivity decreased which was likely due to the decrease in hole mobility. At higher loadings of EBSA, the hole mobility was found to decrease because of the formation of permanent charges, which were supported by the increase in the dielectric constant of the P3HT-EBSA films.[71] Because EBSA significantly improved the hole mobility of P3HT, we also introduced EBSA in a radical polymer system, and the basics of this system will be discussed in the following section.

4.3 Synthesis of poly(2,2,6,6-tetramethylpiperinidyloxyl methacrylate) (PTMA)

First, we present the synthesis of poly(2,2,6,6-tetramethylpiperinidyloxyl methacrylate) (PTMA). In this work, the polymers have been characterized by ^{1}H NMR and ^{13}C NMR spectroscopy to show that the polymer has been synthesized successfully and to determine the polymer tacticity. Size exclusion chromatography (SEC) was used to determine the average molecular weights and dispersity of the polymer. Fourier transform infrared spectroscopy (FT-IR) and electron paramagnetic resonance spectroscopy (EPR) were used to determine the functionality of the pendant groups in the polymers. Differential scanning calorimetry (DSC) was used to determine the glass transition temperature of the polymers.

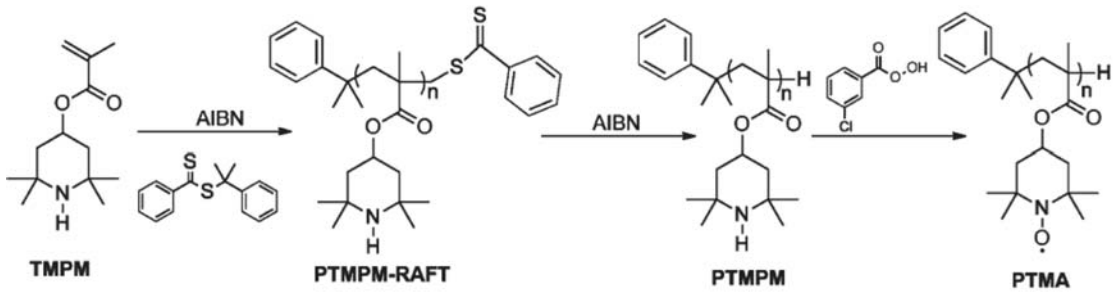

Figure 17. Reaction scheme by which PTMA was synthesized in a controlled manner using RAFT polymerization.

After analyzing the conductivity of a well-studied conjugated polymer, we studied the transport properties of an emerging radical polymer, poly(2,2,6,6-tetramethylpiperinidyloxyl methacrylate) (PTMA). First, we synthesized this polymer by means of reversible addition-fragmentation chain transfer (RAFT) polymerization, as shown in Figure 17.[4] In the first reaction, 2,2,6,6-tetramethyl-4-piperidylmethacrylate (TMPM) was reacted with 2-phenyl-2-propylbenzodithioate (RAFT agent) and 2,2'-azobis(2-methylpropionitrile) (AIBN) to yield the product of PTMPM-RAFT. The

following are conditions for a typical reaction. To a 100 mL reaction vessel containing a Teflon-coated magnetic stir bar, 10 g (0.04 mol) of TMPM, 0.073 g (0.4 mmol) of AIBN, 1.076 mL (4 mmol) of RAFT agent, and 80 mL of toluene were added. Once the solids were dissolved completely in the solvent, three freeze-pump-thaw cycles were performed to remove any dissolved gasses which may have inhibited the reaction. After the last degassing cycle, the reaction flask was refilled with argon. Then, the reaction was heated to 75 °C and stirred for 12 h. To terminate the reaction, the reaction flask was cooled and exposed to air. Subsequently, the solution was transferred to a 100 mL round-bottom flask. The solution was concentrated to about 3 mL using a rotary evaporator. After allowing the mixture to cool to room temperature, the product of PTMPM-RAFT was precipitated in cold hexanes. After filtering, the solid polymer was dried under reduced pressure overnight.

The next reaction involved the removal of the RAFT terminus from the polymer by reacting PTMPM-RAFT with an excess of AIBN in a protic solvent. The following is the procedure of an example reaction. In a 100 mL reaction flask containing a stir bar, 2 g (0.25 mmol) of PTMPM-RAFT, 2 g (12 mmol) of AIBN, and 25 mL of toluene were mixed. Three freeze-pump-thaw cycles was performed and then the reaction flask was refilled with argon. The reaction was heated to 75 °C and stirred. After a reaction time of 12 h, the reaction flask was cooled and exposed to air. Subsequently, the solution was transferred to a 100 mL round-bottom flask. The solution was concentrated to about 1 mL using a rotary evaporator. After allowing the mixture to cool to room temperature, the product of PTMPM was precipitated in cold hexanes. After filtering, the polymer was dried under reduced pressure overnight. The pink color associated with the RAFT

terminus changed to a white color after this reaction due to the removal of the chain transfer end group.

In the last reaction step, PTMPM was oxidized with *meta*-chloroperbenzoic acid (*m*CPBA) to form PTMA. In a vial containing a stir bar, 1 g (5.8 mmol) of *m*CPBA was dissolved in 10 mL of dichloromethane (DCM). In another vial containing a stir bar, 0.5 g (0.13 mmol) of PTMPM was dissolved in 10 mL of DCM. After the materials were well-dissolved in the solvent, the acid was added to the polymer solution and stirred at room temperature. After a controlled reaction time, the combined polymer-oxidizer solution was washed with an aqueous sodium carbonate solution (pH = 13) three times. Then, the polymer in the organic phase was collected and precipitated in hexanes at room temperature. The polymer was dried under reduced pressure overnight. Note that PTMA has an orange color.

A range of molecular weights of PTMA that have been synthesized are $15 \leq M_n \leq 80$ kg mol^{-1} and all polymers have dispersity ($Đ$) values of ~1.3. The molecular weight and dispersity values were determined with size exclusion chromatography against polystyrene (PS) standards. DSC was used to determine the glass transition temperature of PTMA, which was found to be ~175 °C for all samples.

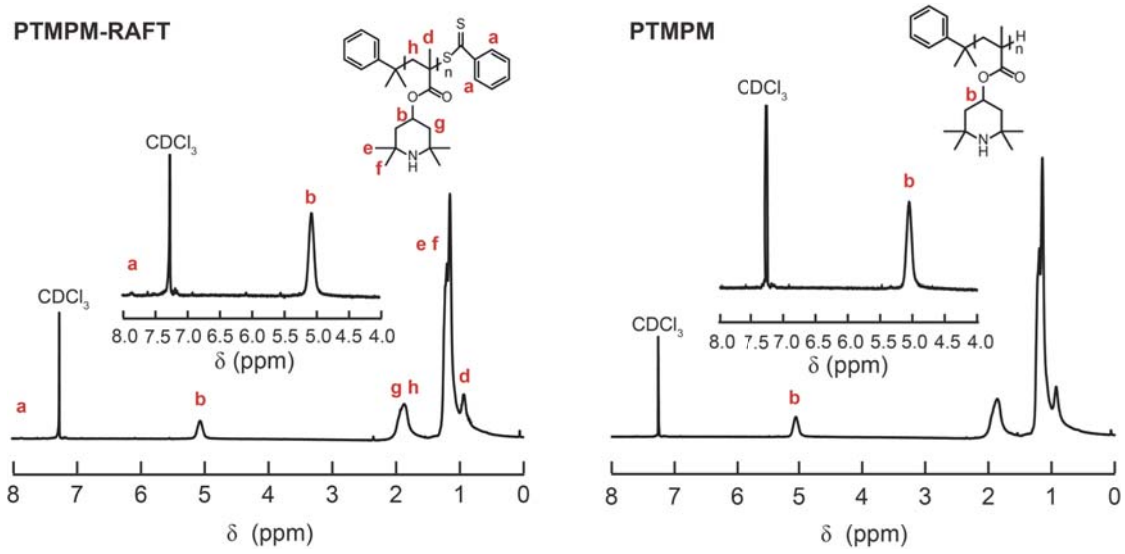

Figure 18. ^{1}H NMR spectrum of PTMPM-RAFT (left) and PTMPM (right). The peak a downfield of the solvent peak highlights the chain transfer end group. The disappearance of peak a in the ^{1}H NMR PTMPM indicates the removal of the RAFT terminus.

In the ^{1}H NMR spectrum of PTMPM-RAFT (Figure 18), the peak a corresponds to the protons associated with the end group of the polymer and peak b corresponds to one proton in a repeat unit of TMPM. Integrating the area underneath the peak allows for an estimation of the number-average molecular weight, which corresponds well with the molecular weight calculated with size exclusion chromatography. The NMR spectrum in the right of Figure 18 demonstrates the removal of the reactive chain transfer end groups from the chains, which is necessary in order to avoid crosslinking during the subsequent oxidation reaction.

Although we synthesized PTMA using a RAFT polymerization methodology, PTMA can be synthesized through many other synthetic routes. For instance, in the work of Lopez-Pena *et al.*, the monomer unit of PTMA was synthesized using group transfer polymerization.[73] In that method, close to 100 % of radical sites in the repeat units were

achieved. Because of the radical sites within the polymer, the nitroxide moiety was quenched with phenylhydrazine to obtain an ^{1}H NMR spectrum at an elevated temperature. In order to analyze the peaks of the methylene groups, the high-field portion of the spectrum was deconvoluted. Thus, with ^{1}H NMR spectroscopy, the tacticity of PTMA was determined to be 84% isotactic through their synthetic route.[73]

Using our polymerization route, the PTMPM tacticity was determined by employing ^{13}C NMR spectroscopy at room temperature in a polymer concentration of 100 mg mL^{-1} in chloroform. Because of the electron-withdrawing nature of the substituent groups, the carbonyl carbons on the same side of the polymer backbone were expected to be more deshielded and shifted downfield than the carbonyl carbons on opposite sides of the polymer backbone, corresponding to rr and mm, respectively (Figure 19). Here, the peaks at 177.5, 176, and 175.5 ppm resemble the peaks at 178, 177, and 176.5 ppm of PMMA found by Ishitake, *et al*..[74] By integrating the areas under the carbonyl peaks, the normalized magnitudes are 62.5, 34.4, and 2.9 which correspond to rr, mr, and mm, respectively. Therefore, through a controlled radical polymerization, the pendant groups mostly alternate from side-to-side on the polymer backbone of PTMA. Consequently, a different tacticity of PTMA can be achieved by utilizing different synthetic routes. This information would be useful for molecular simulations in which the packing density and distance between radical sites are of interest.

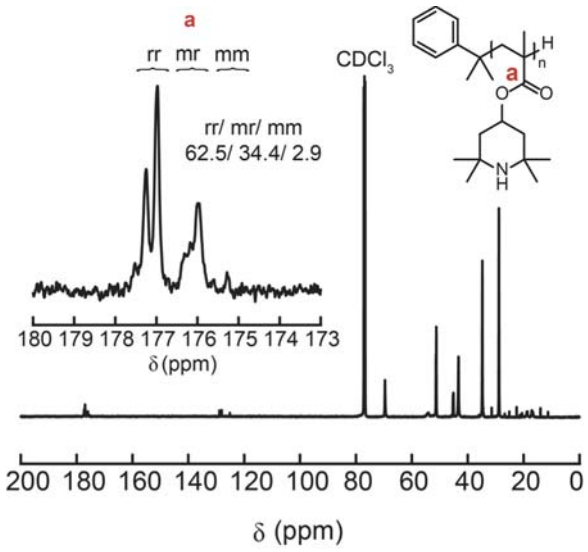

Figure 19. The ^{13}C NMR spectrum of PTMPM, 100 mg mL^{-1} in chloroform at room temperature. The inset shows the chemical shift corresponding to the carbon at the C=O bond, which was used to determine the tacticity of the polymer. Here, r and m represents the chirality (r is racemo and m is meso). Peaks labeled with rr indicates a syndiotactic configuration, mm for an isotactic configuration, and rm for an atactic configuration.

4.4 Doping PTMA with ethylbenzene sulfonic acid (EBSA)

Using the two-point method described previously, the electrical conductivity of PTMA was determined to be on the order of ~10^{-6} S cm^{-1}. In order to improve the electrical conductivity of PTMA, dopants can be introduced into the polymer. Because ethylbenzene sulfonic acid (EBSA) has improved the conductivity of P3HT, we have introduced EBSA to improve the conductivity of PTMA as well. In this work, EBSA was used to dope PTMA by blending the two together overnight in dimethylformamide (DMF). This was done because TEMPO-like units have been shown to disproportionate and convert into oxoammonium salts in the presence of a strong acid.[75]

Similarly, we propose that PTMA interacts with EBSA as shown in the proposed doping mechanism (Figure 20). In a stoichiometric ratio of one EBSA molecule to two radical repeat units of PTMA, the proton on the EBSA interacts with the lone electron on

the oxygen, which result in an anionic form of EBSA and entity A. This anionic form of EBSA is counterbalanced by the oxoammonium cation, entity B. In an equimolar stoichiometric ratio between EBSA and radical repeat units of PTMA, the increase in acidity leads to protonation of the nitrogen atom, thus producing a cationic salt, entity C, and entity B.

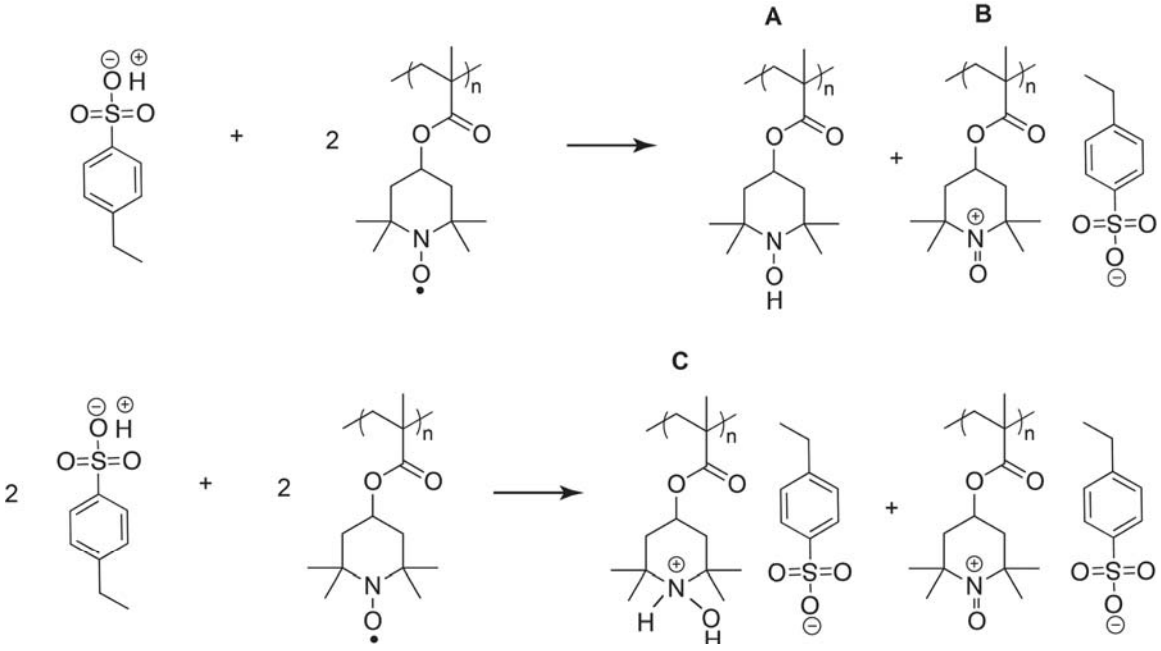

Figure 20. Proposed doping mechanism of EBSA on PTMA based on the stoichiometric ratio of EBSA and PTMA. The acidity of EBSA converts the nitroxide radical to cations, which are balanced by the anionic form of EBSA.

The loss of radical density in PTMA due to EBSA doping was apparent with the formation of salts and the significant decrease in EPR signal. In fact, in a 1:2 molar ratio of TMPM:EBSA, the radical density of PTMA after doping was 0.3% of the radical density before doping. This was calculated by comparing the total absorption intensity in the EPR signal. Therefore, EBSA can lower the radical density of PTMA, which is driving mechanism behind charge transport in radical polymers. However, EBSA can

also increase the cation density, which also affects charge transport. As a result, we expect an optimum amount of EBSA that would enhance the conductivity of PTMA.

After observing films of PTMA using microscopy, it was apparent that poor film quality was an issue, and contributing to the low conductivity values observed (Figure 20). When the PTMA film (~300 nm) was spun-coat on top of a glass substrate, the film contained a relatively fair amount of fractures. However, when the film (~ 1 μm) was drop-casted onto a glass substrate, the film visibly-contained many fractures and it would delaminate from the glass substrate. By introducing EBSA into system, it was noticeable that the film quality was improving, as shown in the case of a 32.5 wt% loading of EBSA (Figure 21). However, at high EBSA loading (>60 wt% EBSA), the polymer matrix is in the liquid state at room temperature. This is due to the plasticizing effect of EBSA (T_g ~ –20 °C).

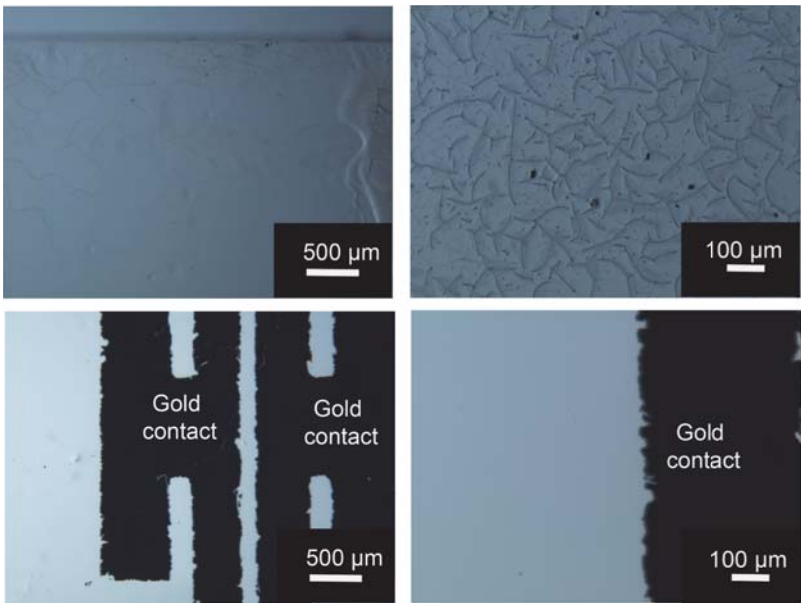

Figure 21. Top left: PTMA (100 mg mL^{-1}) spun-coat from DMF and annealed for 20 m at 130 °C. Top right: PTMA (20 mg mL^{-1}) drop-casted from chloroform. Bottom row: PTMA (20 mg mL^{-1}) and EBSA (32.5 wt%) drop-casted from DMF and annealed for 20 m at 130 °C.

Because the EBSA seemed to plasticize the films, the thermal transitions of the composite materials were analyzed. The glass transition temperatures were determined by examining the heat uptake utilizing DSC. As the amount of EBSA increased, the glass transition temperature (T_g) of the polymer matrix decreased (Figure 22). Specifically, the glass transition temperature data were fit to the Fox and Allen equation (Equation 4.3) and the Gordon-Taylor (Equation 4.4 and 4.5). Here, T_g is the glass transition temperature of the system, X_1 is the mass fraction of the plasticizer (*e.g.*, EBSA), X_2 is the mass fraction of the host polymer, and V_i is the specific volume occupied by component *i* at its glass transition temperature, $\Delta\alpha_i$ is the difference of thermal expansion coefficient between the glassy and rubbery state of component *i* at its glass transition temperature, and *k* is the factor that accounts for the polymer's influence on the behavior of the system.[76,77]

$$\frac{1}{T_g} = \frac{X_1}{T_{g1}} + \frac{X_2}{T_{g2}} \tag{4.3}$$

$$T_g = \frac{X_1 T_{g1} + kX_2 T_{g2}}{X_1 + kX_2} \tag{4.4}$$

$$k = \frac{V_2 \Delta\alpha_2}{V_1 \Delta\alpha_1} \tag{4.5}$$

Using the Gordon-Taylor equation, the *k* parameter was determined using the least-squares method to be 1.35 (Figure 23). A *k* parameter less than 1 indicates that the plasticizer has a large effect on the T_g of the host polymer, while $k = 1$ would correspond to Taylor's relation where the interactions are intermediate between the two components.[76,77] The data fit well at plasticizer compositions of less than 50 wt%. Beyond this loading, the glass transition plateaus at the glass transition temperature of EBSA. At

this loading and above, it is apparent that the polymer matrix is in the form of a gel and not a solid at room temperature.

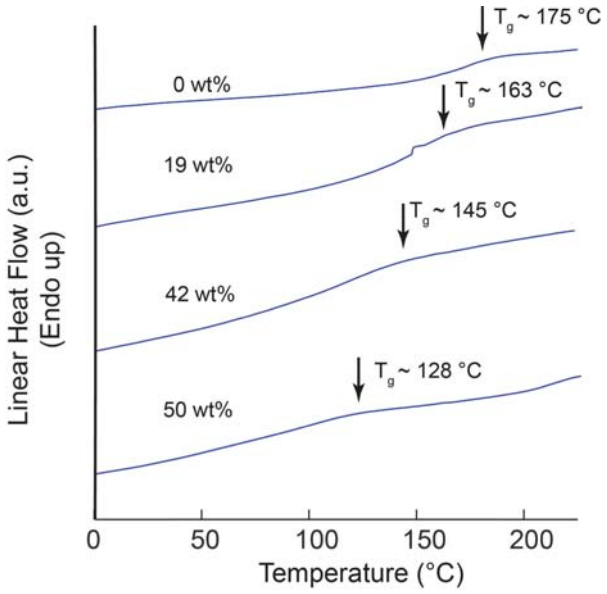

Figure 22. DSC curves of PTMA and EBSA blend. Curves are labeled with the EBSA loading. The glass transition temperature of the polymer matrix decreases as a function of EBSA loading.

In order to measure the conductivity of the polymer matrix, metal contacts were thermally evaporated onto cleaned glass substrates. Then, the polymer blend, which was dissolved in DMF, was drop-casted on top of the substrates, and annealed for 20 m at 130 °C. The film conductivity values were measured using a two-point method. As shown in Figure 23, an increase in polymer conductivity was found only at a doping of about 40 wt%. The conductivity appears to increase with a decrease in glass transition temperature. It is not clear how effective EBSA is as an electrical dopant because the increase in conductivity can be due to: 1) an improvement in film quality; 2) the intrinsic ionic conductivity of EBSA; and/ or 3) the p-type doping of PTMA by EBSA. Nonetheless, it is promising that molecular dopants can increase the electrical conductivity of PTMA by two orders of magnitude.

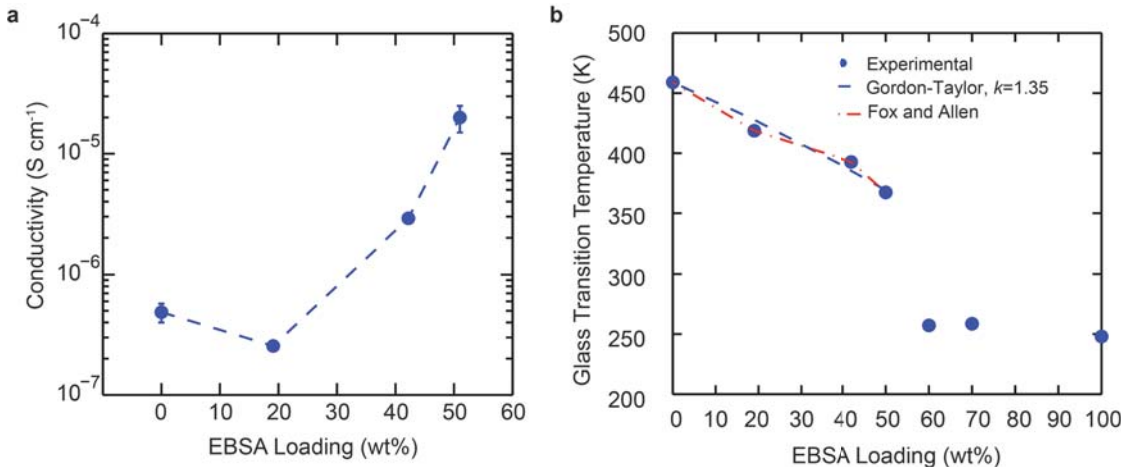

Figure 23. PTMA was dissolved in DMF and EBSA was used as a dopant. a. The electrical conductivity of the EBSA doped PTMA films. b. The glass transition temperature of the EBSA doped PTMA films. At 50 wt% EBSA loading and less loadings, the data fit well with the Gordon-Taylor and Fox and Allen equations. At higher EBSA loadings, the glass transition temperature of the blend plateaus at the glass transition temperature of EBSA.

Because of the intrinsic ionic conductivity of EBSA, we hypothesized that the incorporation of organic dopants at an intramolecular level would lead to improvements in transport properties that were more characteristic of the polymer system. In other words, we proposed a method to incorporate dopants within the polymer chain by synthesizing a PTMA-based copolymer with sulfonic functional repeat units, vinyl sulfonate-sodium (VS).

4.5 Synthesis of intramolecular dopants in radical polymers (PTMA-*co*-PVS)

A free radical copolymerization of poly(2,2,6,6-tetramethyl-1piperinidyloxy-4-yl methacrylate)-*co*-poly(vinyl sulfonate-sodium) PTMA-*co*-PVS occurs through the modified reaction scheme shown in Figure 24.[78] In the first reaction, 2,2,6,6-tetramethyl-4-piperidylmethacrylate (TMPM) reacted with vinyl sulfonate sodium (VS), which was purified with a basic alumina column, using 2,2'-azobis(2-methylpropionitrile) (AIBN)

as an initiator to yield the product of PTMPM-*co*-PVS. In an example reaction, 10.14 g (0.045 mol) of TMPM, 13.3 mL of 25 wt% aqueous VS (0.03 mol), 0.1232 g (0.75 mmol) of AIBN, 24 mL of distilled water, and 38 mL of methanol were added to a 100 mL reaction vessel containing a Teflon-coated magnetic stir bar. Once the solids dissolved completely in the solvent, three freeze-pump-thaw cycles were performed to remove any dissolved gasses, which may inhibit the reaction. After the last degassing cycle, the reaction flask was refilled with argon. Then, the reaction was heated to 55 °C and stirred for a controlled reaction time. To terminate the reaction, the reaction flask was cooled and exposed to air. Because the product precipitates in the reaction, the remaining solution was poured out of the reaction flask and the precipitates were filtered. The precipitates were rinsed with an equivolume of methanol and water three times. After filtering, the polymer was dried under reduced pressure overnight. The ^{1}H NMR spectrum confirmed the formation of the copolymer (Figure 25).

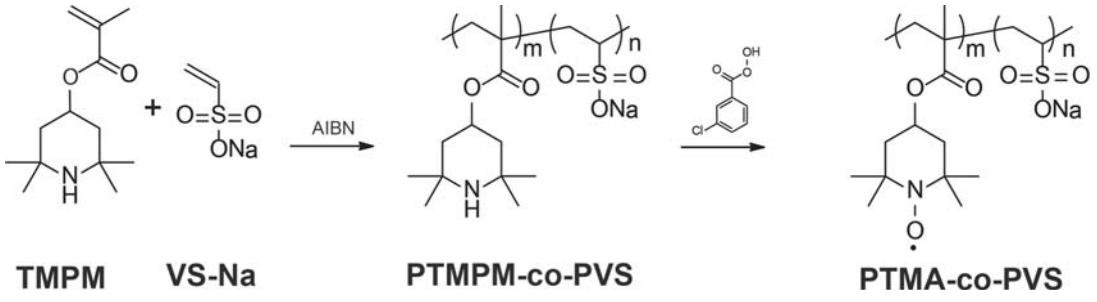

Figure 24. Modified reaction scheme of the free radical copolymerization of PTMA-*co*-PVS.[78]

In the last portion of the reaction, PTMPM-*co*-PVS was oxidized with *meta*-chloroperbenzoic acid (*m*CPBA) to form PTMA-*co*-PVS in a ratio of 1 mol TMPM: 3 mol *m*CPBA. For a copolymer containing 38.2 % on a molar basis of VS, 1.686 g of PTMPM-*co*-PVS was dissolved in 56 mL of dichloromethane in a beaker with a stir bar.

In another beaker with a stir bar, 2.39 g (13.8 mmol) of *m*CPBA was dissolved in 56 mL of dichloromethane. After the materials were well-dissolved in the solvent, the acid was added to the copolymer solution and stirred at room temperature. After a controlled reaction time, the combined copolymer-oxidizer solution was washed with an aqueous sodium carbonate solution (pH = 13) three times. Then, the copolymer in the organic phase was collected and precipitated in hexanes at room temperature. The copolymer was dried under reduced pressure overnight.

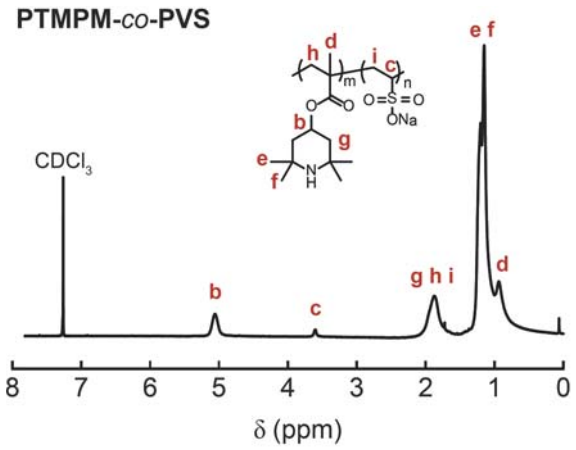

Figure 25. ^{1}H NMR of copolymer (PTMPM-*co*-PVS) by free radical polymerization of TMPM and VS-Na following the methodology described in the literature. Integration indicates 16 TMPM: 1 VS-Na.

4.6 Monomer reactivity of PTMA-*co*-PVS

Using the Finemann-Ross method, the reactivity ratios are deduced as r_1 ~7 and r_2 ~0 where r_i is the ratio of rate constant of a chain ending with repeat unit *i* reacting with monomer *i* divided by the rate constant of a chain ending with repeat unit *i* reacting with a different monomer. In this experiment, *1* refers to TMPM and *2* refers to VS (Figure 26). Considering that r_1 is very large, this indicates that the copolymer consists mostly of TMPM and TMPM tends to self-polymerize. Since r_2 is close to 0, VS does not tend to

self-polymerize. VS is an ionic monomer, which repels itself. Thus, cross-polymerization is preferred. The copolymer structure can be visualized as a polymer chain consisting mostly with TMPM and sporadically with VS molecules. For copolymers, the reactivity ratio also can be deduced with ^{13}C NMR. However, after investigating the carbon NMR of the homopolymer and copolymer, it appears that this strategy is not possible because the carbons in the backbone are very similar. The chemical shift in the carbons cannot be differentiated easily. Therefore, the reactivity ratio was only determined empirically.

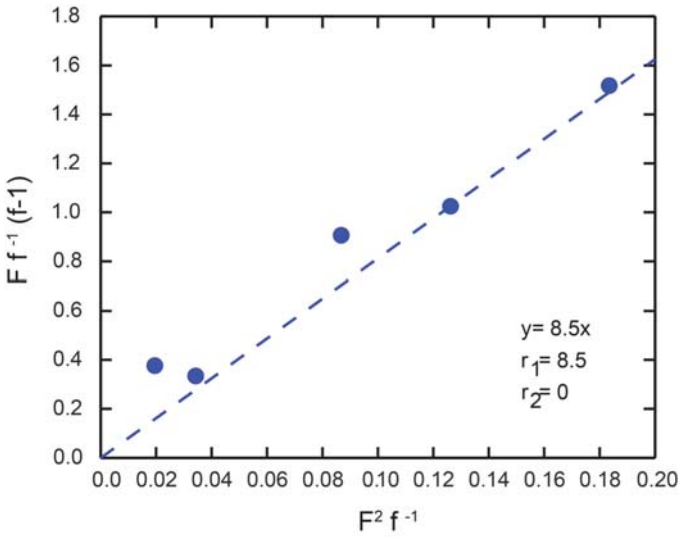

Figure 26. Determination of reactivity constants using the Finemann-Ross method. Here, r_i is the ratio of rate constant of a chain ending with repeat unit *i* reacting with monomer *i* divided by the rate constant of a chain ending with repeat unit *i* reacting with a different monomer. The index *1* refers to TMPM and index *2* refers to VS.

4.7 VS content in PTMA-*co*-PVS as a function of reaction conditions

In order to tune the copolymer to a desired chemical composition, we investigated how the copolymer composition varies with reaction time and monomer composition. We conducted several experiments to measure the final copolymer composition against reaction time (Figure 27). It is important to note that VS is soluble in the aqueous phase

while TMPM is soluble in organic solvents. Because of the different solubility properties of the monomers, as the polymer chain grows, it precipitates out of the reaction, which contains an equivolume of methanol and water. This makes it difficult to obtain kinetic data about the polymer chain in the same reaction. In other words, it is necessary to conduct separate reactions for determining the polymer composition as a function of time while keeping the initial polymerization conditions constant such as the initial monomer composition at an equimolar concentration of TMPM and VS.

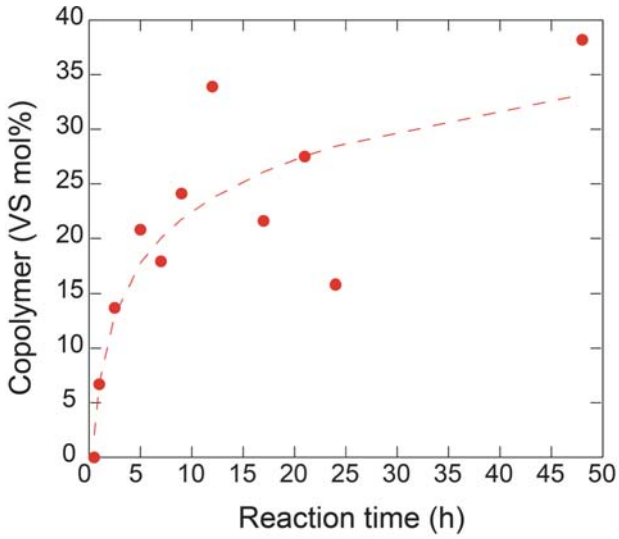

Figure 27. PTMPM-*co*-PVS composition as a function of reaction time. The initial monomer composition contain an equimolar concentration of TMPM and VS. The dashed line serves only as a guide to the eye.

After about half an hour, VS monomer begins to add onto the copolymer chain, as shown in Figure 27. As the reaction time proceeds, more VS monomer adds onto the copolymer chain, which increases the overall VS polymer composition. This occurs as TMPM monomer is used up in the reaction. After about 12 h, the copolymer composition plateaus at a value of 25-30% on a molar basis. At this point, the propagating chains are so large that termination dominates the reaction and equilibrium is reached.

Next, we investigated the copolymer composition as a function of initial monomer composition at two different reaction times, 5 h and 11 h (Figure 28). As we increased the initial VS monomer composition to 50 mol%, the VS composition in the copolymer also increased. However, when we increased the initial VS monomer composition beyond 50 mol%, the VS content in the copolymer actually decreased. This trend was apparent for both the 5 h and 11 h reaction times. This was not anticipated. However, PVS homopolymer was found in the solution of the reaction. Only the solid copolymer contents were analyzed in Figure 28.

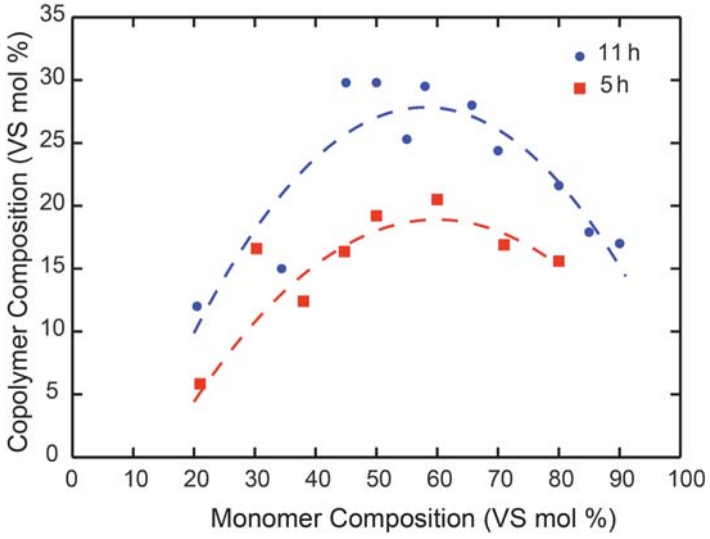

Figure 28. PTMPM-*co*-PVS composition as a function of monomer composition at a 5 h and 11 h reaction time.

To investigate whether a higher VS copolymer content can be achieved, we attempted to synthesize a block polymer with the first block as PVS and second block as PTMPM. In a reaction flask, VS monomers reacted at 55 °C for 3 h, and then a solution containing TMPM monomers were injected in an air-free environment. This was reacted for an additional 16 h. After terminating the reaction, we analyzed the products and found

homopolymer PVS and homopolymer PTMPM. This suggests that when the PVS chains are large, TMPM does not add onto the PVS block. Furthermore, others have found that the vinyl sulfonate-sodium can only be synthesized to a low molecular weight ~4000 g mol^{-1}, about 31 repeat units per chain.[70] This suggests that it is not kinetically favorable for PVS to grow any larger, with VS monomers or any other monomers (*e.g.*, TMPM). From these results, we propose the growth of chains as shown in Figure 29.

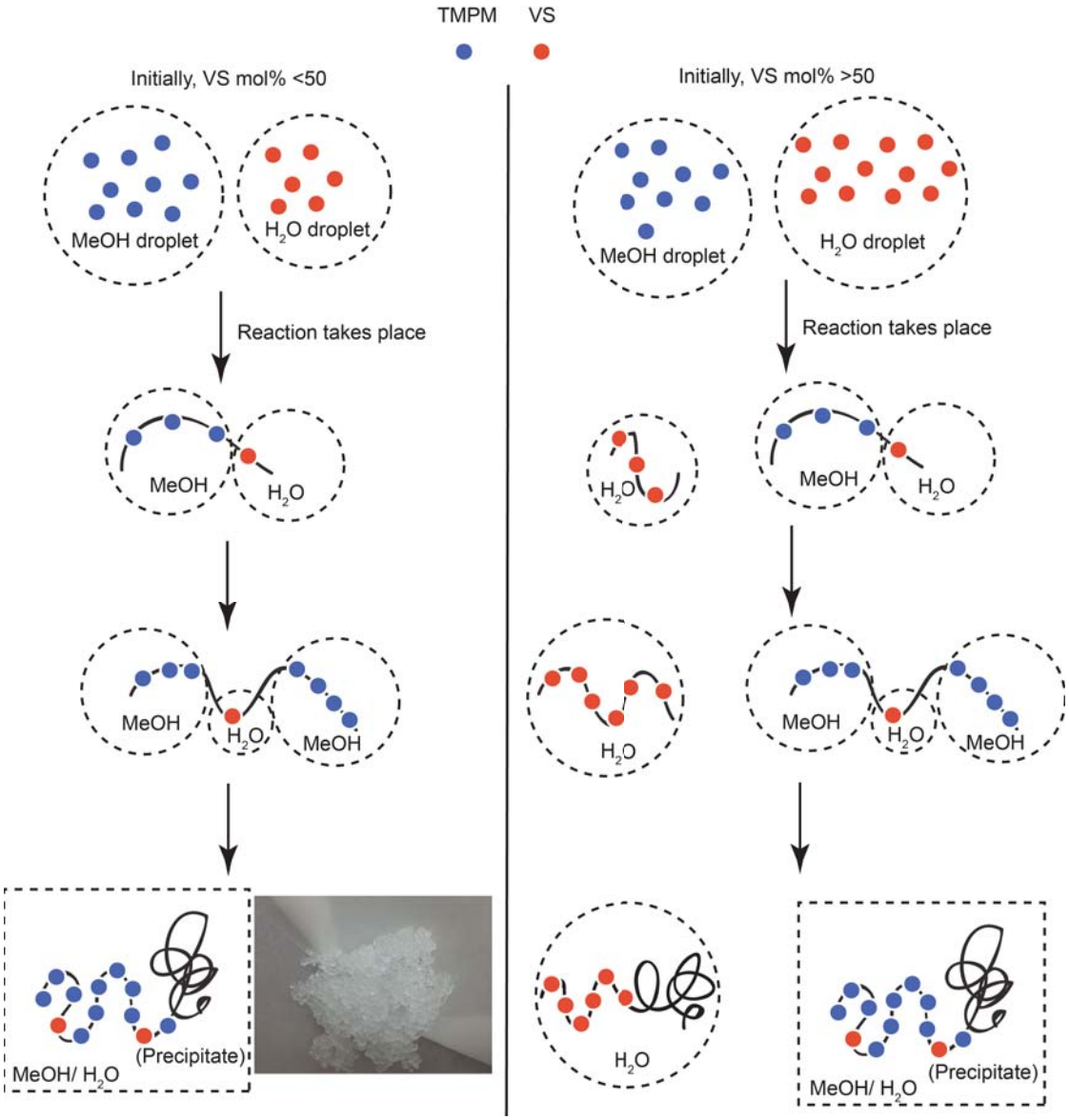

Figure 29. Depiction of the proposed synthesis of PTMPM-*co*-PVS at a low concentration(< 50 mol%) and high concentration (>50 mol%) of VS that is initially in the reactor flask. The dashed circles represent liquid droplets. TMPM monomers are dispersed in methanol droplets and VS monomers are dispersed in water droplets. At a low VS concentration, the copolymer becomes a certain length at which it precipitates out of the media. At a high VS concentration, the copolymer is formed but, due to the hydrophilicity of PVS, PVS homopolymer is also formed in the aqueous phase. The photo shows the copolymer precipitate that has been filtered from the media.

4.8 Functionality of TMPM in PTMA-*co*-PVS (12 mol% PVS)

After studying the copolymerization reaction, we monitored the oxidation reaction of functionalizing PTMPM-*co*-PVS to PTMA-*co*-PVS. The duration of the oxidation reaction is very important because it influences the concentration of radical sites and cation sites in the copolymer, which affects charge transport. Therefore, PTMPM-*co*-PVS (12 mol% PVS) was oxidized for different lengths of time, ranging from 0.5 h to 3 h. Beyond 3 h, the copolymer formed a gel in solution. In Figure 30, the FT-IR spectrums of the copolymer in the solid state were normalized to the C-H stretch at about 3000 cm^{-1}. The cation band occurs at a wavenumber of 1540 cm^{-1} and the radical band occurs at a wavenumber of 1460 cm^{-1}.[79]As the reaction proceeded, the cation stretch increased. At 2 h oxidation, the cation band was at a relative maximum. Beyond this, the cation stretch was hardly noticeable. Because the radical band overlaps with another band, it is difficult to analyze the relative intensity of the radical content. However, the radical electron density can be measured using electron paramagnetic resonance, EPR.

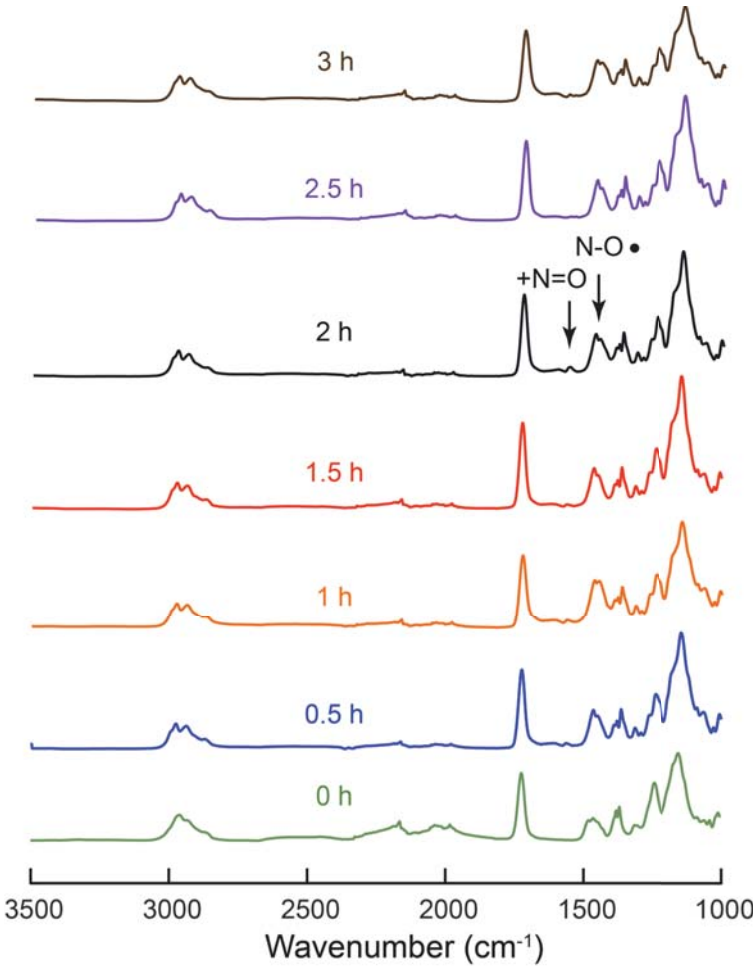

Figure 30. FT-IR of PTMA-*co*-PVS (12 mol% PVS) at various lengths of oxidation time.

In EPR, the first derivative of the absorption of the radical sites is plotted against the magnetic field (Figure 31). By integrating the first derivative and calculating the area underneath the absorption peak, the total absorption intensity was measured. A calibration curve using PTMA as a reference has been generated to correlate the molar concentration of radical units and total absorption intensity of the spectrum (Figure 32). In this experiment, TEMPO could not be used as the calibration standard because TEMPO is known to form dimers at the radical sites in the solution state.[80] Because TEMPO forms dimers, the EPR absorption signal is lowered. Considering that PTMA is

a bulky polymer, dimers are less likely to form when compared with TEMPO molecules. Therefore, the radical units in PTMA are a more accurate representation of the radical units in PTMA-*co*-PVS. The copolymer was dissolved in chloroform at a concentration of 2 mg mL^{-1}. Because the copolymer contains 12 mol% VS, we accounted for this when we determined the molar concentration of radical units in Equation 4.6. Here, w is the concentration of copolymer in mg mL^{-1}, m_{VS} is the molecular weight of VS monomer in mg $mmol^{-1}$, m_{TMPM} is the molecular weight of TMPM monomer in mg $mmol^{-1}$, and C is the concentration of PTMA in mmol mL^{-1}.

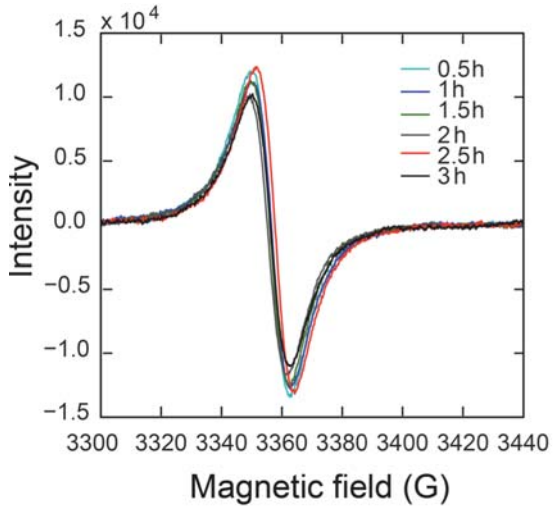

Figure 31. First derivative of the absorption signal in EPR of PTMA-co-PVS (12 mol% PVS) at various lengths of oxidation time.

$$C = \frac{w}{0.12m_{VS} + 0.88m_{TMPM}} \tag{4.6}$$

Using the concentration of PTMA and the calibration equation (Equation 4.7), a theoretical maximum radical total absorption intensity was computed. Here, A is the total absorption intensity and C is the concentration of radical units in PTMA in mmol mL^{-1}.

$$A = 6x10^{10}C \tag{4.7}$$

From this, we were able to calculate the percent of TMPM that is in the radical state. We found that a maximum of 30% TMPM in the copolymer was oxidized. After 1 h of oxidation, the radical density decreases which is likely due to cross-linking.

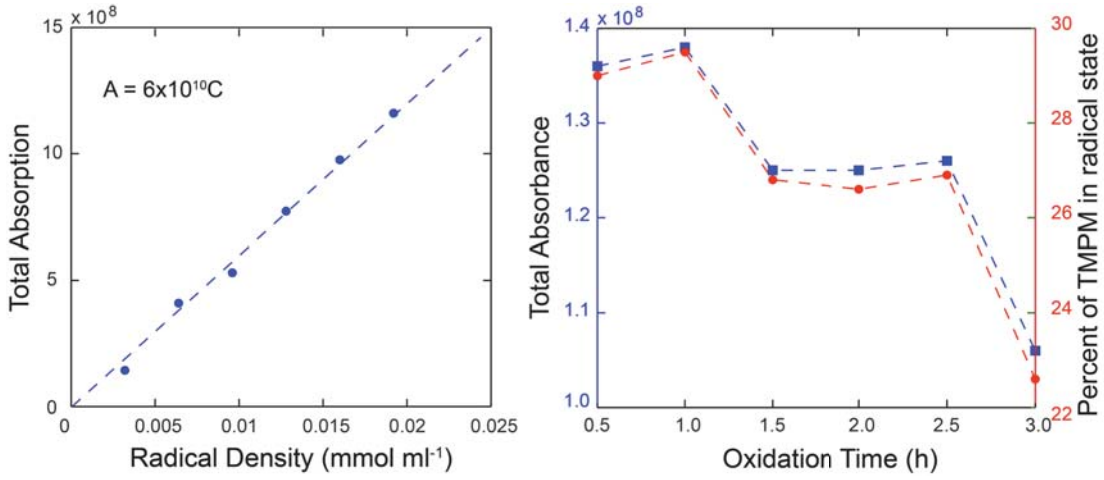

Figure 32. Left: Calibration curve of radical concentration versus total absorption intensity using EPR. Right: Left axis is the total absorption intensity of PTMA-*co*-PVS (12 mol% PVS) at various lengths of oxidation time. Right axis is the calculated amount of TMPM in the copolymer that exists in the radical state.

From FT-IR and EPR, it is apparent that the radical density maximizes at a 1 h oxidation time and the cation maximizes at a 2 h oxidation time. Previously, it has been determined that different lengths of oxidation times of PTMPM lead to different concentrations of pendant group functionalities.[79] At shorter oxidation times, radical sites are formed. As oxidation proceeds, cation sites are formed. At longer oxidation times, protons begin to attack the lone electrons at the oxygen atoms, thus, N-OH pendant groups are formed.[79] Similar to the change in functionality of PTMA pendant groups due to the length of oxidation time, in PTMA-*co*-PVS, a similar change in functionality takes place. We hypothesize that after 1 h of oxidation, cations form, such that the radical density starts to decrease, as determined by EPR. After 2 h of oxidation, N-OH forms,

such that the cation density begins to decrease, as determined by FT-IR. After analyzing the molecular structure and functionality of the PTMA-*co*-PVS, its transport properties were studied.

4.9 Hole mobility of PTMA-*co*-PVS (12 mol% PVS) as a function of oxidation time

The Mott-Gurney law can be used to determine the material's hole mobility.[81,82] There are several assumptions that allow the Mott-Gurney law to be applicable: the diffusion current in the semiconductor is negligible, mobility is not affected by the electric field, and the bulk material has a negligible amount of traps. When the applied voltage is increased to the point where the injected holes become more than the intrinsic holes in the material, the flow of current changes. When this occurs, the device is behaving as a "space charge-limited" device.[81,82]

Devices were made with the copolymer spin-coated on top of ITO on glass substrates. Then, aluminum was thermally evaporated onto the films. A small amount of silver paste was added on top of the aluminum to prevent piercing through the devices during testing. Using the Lakeshore and Keithley, a voltage (V) was applied from 0 to 8 V, with Al as the ground electrode. The current density (J) was measured and plotted as a function of V (Figure 33). Then, the voltage was applied in the opposite direction. It is interesting to note that the forward and reverse J-V sweeps lack hysteresis. This indicates that the copolymer may be able to transport electrons just as well as holes. This will be investigated in the future works. We used the Mott-Gurney relationship to calculate the hole mobility from this data. By taking the log of the voltage and the log of the current density, we can look for the regime at which the copolymer is acting as a space charge-

limited device. In a space charge-limited device, the current density is proportional to the voltage squared (Equation 4.8). Here, μ is the carrier mobility, ε_o is the dielectric constant, ε is the permissivity constant, and L is the film thickness.

$$\mu = \frac{8\varepsilon\varepsilon_o JL^3}{9V^2} \tag{4.8}$$

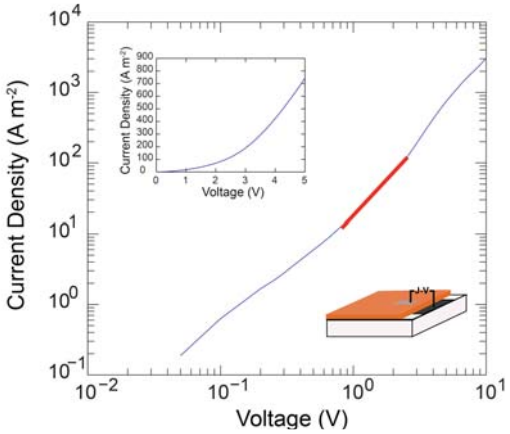

Figure 33. Voltage versus current density curve of a Al-PTMA-ITO on glass substrate device. The red line represents the regime at which the device is a space-charge limited device. The inset shows the geometry of the device, where a current density- voltage sweep is collected between the top aluminum contact and bottom ITO contact.

The space charge-limited regime was found at voltages less than 3.5 V. As shown in Figure 34, the carrier mobility does not vary much with oxidation time but it maximizes at a 1.5 h oxidation time. This corresponds to a copolymer that contains radical and cation functional groups, as previously determined with FT-IR and EPR. Furthermore, the carrier mobilities at less optimal oxidation times of the copolymer were close to the carrier mobility of PTMA. While VS may p-type dope PTMA, this did not improve the carrier mobility of PTMA significantly. This may be due to the fact that the oxidation reaction already p-type dopes PTMA by increasing the cation concentration in

PTMA. Thus, any improvements in carrier mobility may be due to the ionic character of the VS repeat units.

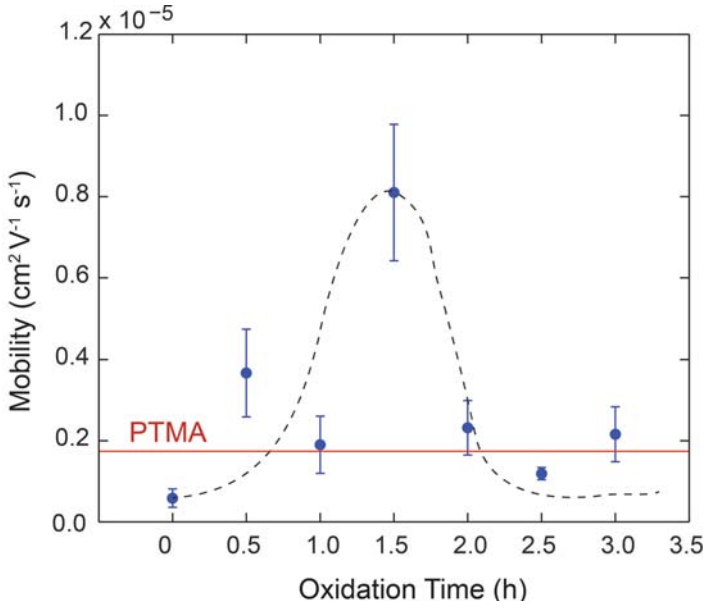

Figure 34. Hole mobility of PTMA-*co*-PVS (12 mol% PVS) at various oxidation times. Each data point represents 7-12 devices.

4.10 Temperature-dependent hole mobility of PTMA-*co*-PVS (12 mol%)

The devices used to measure the carrier mobility of the copolymer at 1.5 h oxidation time were heated and cooled to measure the temperature-dependent hole mobility. Although the mobility does not vary significantly with temperature, there are two slight trends (Figure 35). At temperatures below 333 K, the mobility increases with an increase in temperature, which is consistent with hopping transport. At temperatures above 333 K, mobility decreases with an increase in temperature, which suggests that scattering is playing a large role in reducing the carrier mobility.

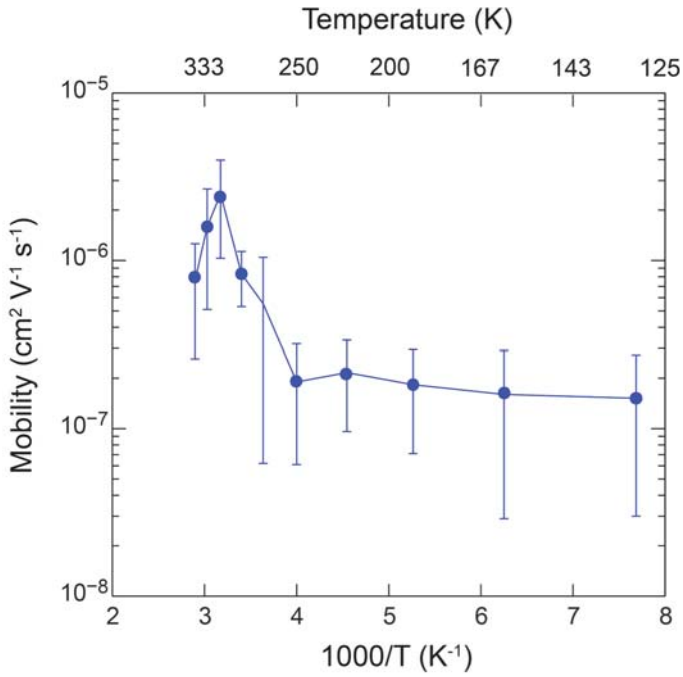

Figure 35. Temperature-dependent hole mobility of PTMA-*co*-PVS (12 mol% PVS). 11 devices were analyzed for each data point. The mobility was calculated using space-charge limited devices. The solid line serves only to guide the eye.

By incorporating dopants within PTMA, we have improved the hole mobility from a pristine PTMA system. The peak hole mobility for PTMA-*co*-PVS (12 mol% PVS) occurred at a value corresponding to a copolymer oxidation time of 1.5 h. At this oxidation level, cations and radical sites (27 mol% of the total moles of TMPM) are present in the copolymer. Ultimately, fine-tuning of copolymer's functionality enables the optimization of the copolymer's transport properties, and, thus enhances its ability to serve as a conductive material in electronic applications.

5. FUTURE WORK

5.1 RAFT-mediated polymerization of PTMA-*co*-PVS

After tuning the VS copolymer composition and functionality of the copolymer to optimize the transport properties of PTMA-*co*-PVS, we plan to determine the effect of molecular weight on the copolymer's transport properties. In order to control the molecular weight, RAFT-mediated polymerization can be used to synthesize the copolymer (Figure 36). In our preliminary results, we have synthesized the copolymer, as confirmed with ^{1}H NMR (Figure 37). In the ^{1}H NMR spectrum, peak a represents a proton on the reactive chain transfer end group. The disappearance of peak a in the ^{1}H NMR spectrum of PTMPM-*co*-PVS indicates the removal of the reactive end group, which is necessary to avoid crosslinking during the subsequent oxidation reaction (right of Figure 37). Peak b and c represents a distinctive proton on a repeating unit of TMPM and VS, respectively. By integrating peaks b and c, the copolymer composition can be determined.

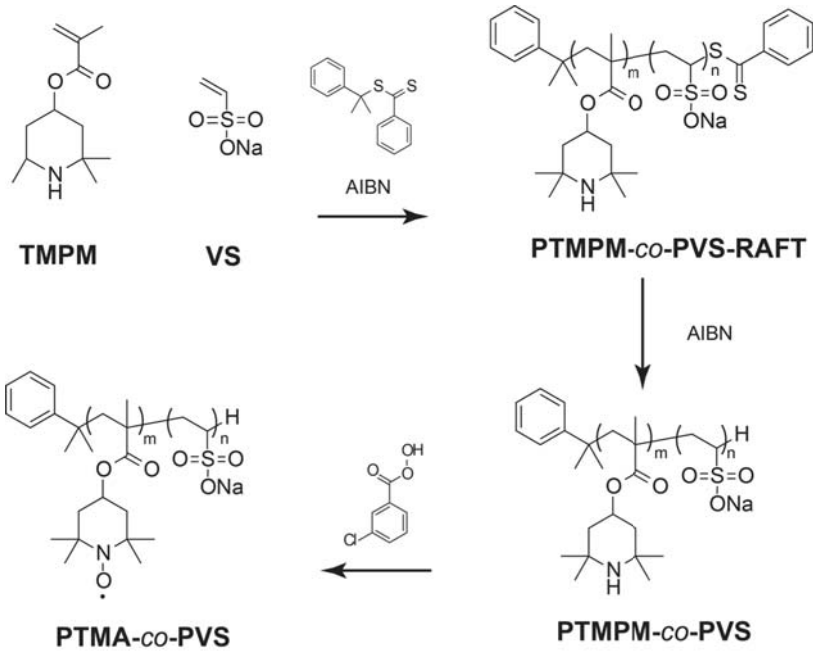

Figure 36. RAFT-mediated polymerization synthesis route to produce PTMA-*co*-PVS.

In an example reaction, 0.9013 g (4 mmol) of TMPM, 0.44 ml (1 mmol) of an aqueous solution of VS, 8.2 mg (0.05 mmol) of AIBN, and 19 μL (0.06 mmol) of RAFT reacted for 5 h at 55 °C in an air-free environment. This resulted in a copolymer composition containing 43 mmol of TMPM per mmol of VS. Using ^{1}H NMR, the copolymer has an average molecular weight of ~12 kg mol^{-1}. By controlling the molecular weight and measuring the transport properties of the copolymer, structure-property relationships can be determined.

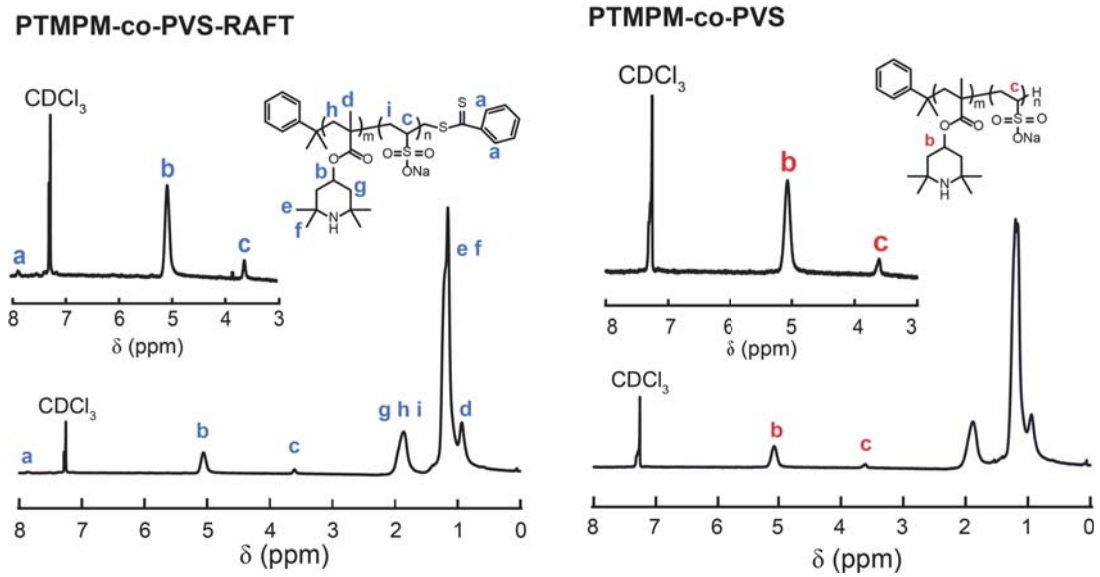

Figure 37. Controlled polymerization of TMPM and VS using a RAFT agent. Left: ^{1}H NMR spectrum of PTMPM-*co*-PVS-RAFT). Right: ^{1}H NMR spectrum of copolymer PTMPM-*co*-PVS indicating the removal of the RAFT end group. Integration indicates 43 TMPM: 1 VS. Here peak a corresponds to two protons on the RAFT terminus, peak b corresponds to a distinctive proton on a TMPM repeating unit, and peak c corresponds to a distinctive proton on a VS repeating unit.

5.2 Blending PTMA with PVS

The copolymer synthesis results show that it is difficult to acquire a high content of VS. That is, the highest achieved by our team was 38 mol% VS. However, if a higher VS content was achieved, the transport properties of the system may be improved. If synthesizing a higher VS content is not possible, it is possible to achieve a higher concentration of VS in the thin film simply by blending the two homopolymers. In our preliminary results, we synthesized PVS with AIBN as the initiator using free radical polymerization. The impurities in the VS monomer were difficult to remove from PVS. In the polymerization of PTMPM-*co*-PVS, this problem was circumvented because the copolymer does not dissolve in water but the impurity does. To remove the impurities, we have attempted to extract the polymer with THF and methanol. While this reduced the

amount of impurities, the impurities were still present (Figure 38). To improve the purity of the polymer, we utilized a cellulose dialysis tubing, Sigma-Aldrich D2272, with an average flat width of 9 mm. The porous tubing is useful in separating compounds with a molecular weight greater than 2,000 g mol^{-1} and compounds with a molecular weight lower than 1,200 g mol^{-1}. The polymer was dissolved in distilled water and injected into the dialysis tubing. After immersing the dialysis tubing in distilled water for a day, the polymer was recovered and dried. Figure 38c confirms the removal of the impurities by means of the dialysis tubing. In the ^{1}H NMR of Figure 38c, the presence of peak e and d indicates that the polymer terminated by disproportionation and formed the vinyl protons corresponding to the peaks. By integrating the peaks, we determined that the PVS has an average molecular weight ~2,500 g mol^{-1}. With the materials synthesized, the next step is to optimize the fabrication of blending the two polymers. Then, we will measure the transport properties and examine the film quality with microscopy.

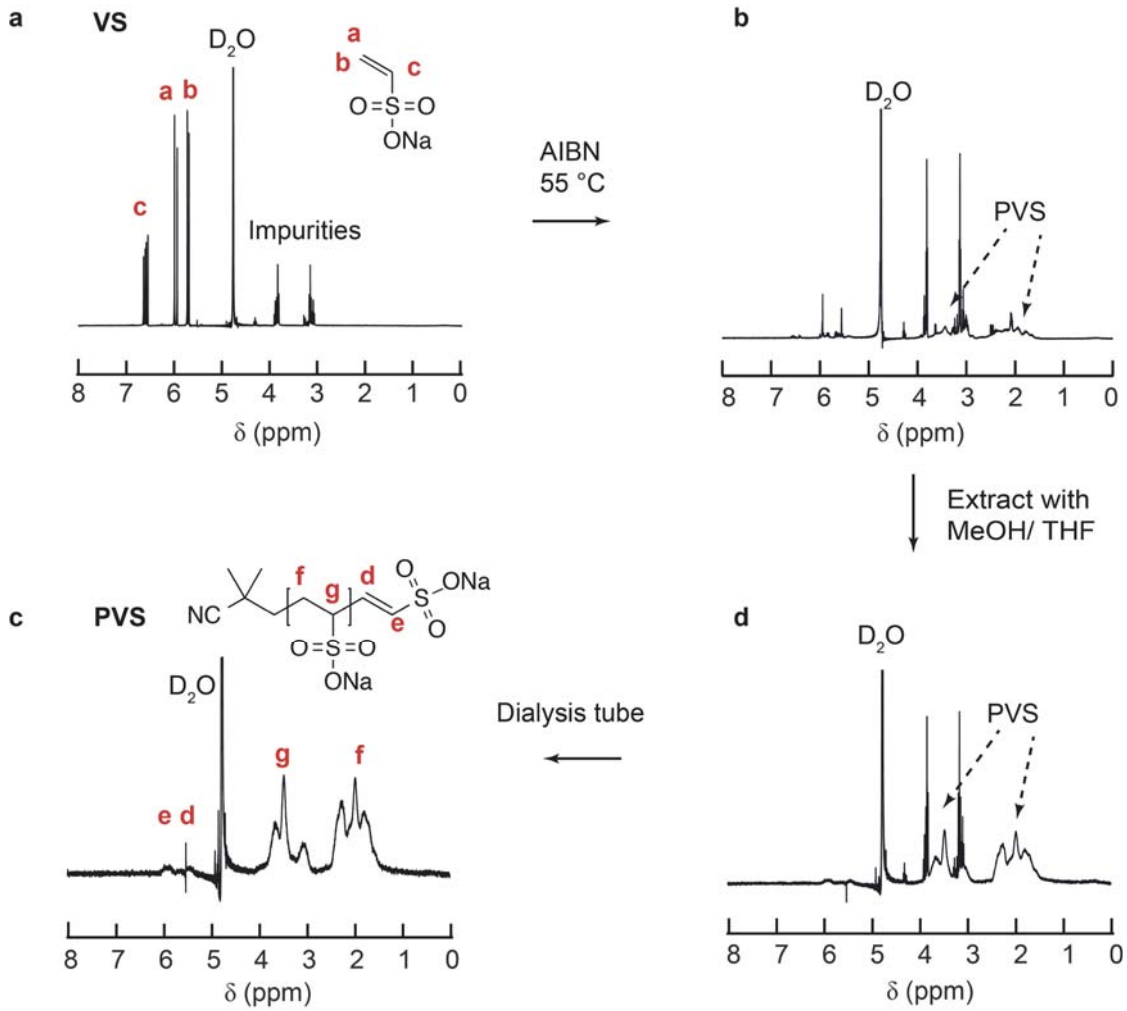

Figure 38. a. ^{1}H NMR spectrum of the VS monomer which contained impurities. b. ^{1}H NMR spectrum of PVS with residual monomer and impurities. c. ^{1}H NMR spectrum of the polymer after solvent extraction, which shows the removal of monomers and reduction of impurities. d. ^{1}H NMR spectrum of the polymer after being in a dialysis tube immersed in distilled water, which shows the removal of the impurities. The proton peaks in the vinyl region indicate that the polymer terminated by disproportionation.

5.3 Determining the electron transport in PTMA-*co*-PVS

In this work, we focused on the hole transport of PTMA-*co*-PVS. However, PTMA-*co*-PVS is expected to transport electrons as well as holes. This is characteristic of radical polymers because radical polymers undergo a reversible oxidation-reduction reaction. In an extreme case, when the copolymer is functionalized to contain all cation

pendant groups, it is expected to transport electrons well. Thus, it may be considered an ambipolar material. It would be very interesting if the functionality of the copolymer can be tuned in such a way that allows it to switch from being a p-type to an n-type material. Therefore, we will measure the electron mobility and Seebeck coefficient of the copolymer as a function of the radical and cation density.

5.4 Determining the thermoelectric properties of PTMA-*co*-PVS

The Seebeck coefficient of the polymer thin film is not only useful in determining with the copolymer is p-type or n-type, but it is also useful for determining the thermoelectric power factor (σS^2). Using a device, containing a thin-film of polymer on top of glass substrates with metal contacts at the corners of the film, the voltage generated can be measured across the film in the presence of a temperature gradient and the Seebeck coefficient can be calculated (Figure 39). The electrical conductivity can be measured as described in the previous section or using the van der Pauw method.[83,84] The power factor describes the electrical component of the thermoelectric figure of merit for a material. By utilizing the molecular structure studies in this work and measuring the thermoelectric properties of the copolymer, we can systematically tailor the functionality of the copolymer to function more effectively as a thermoelectric material.

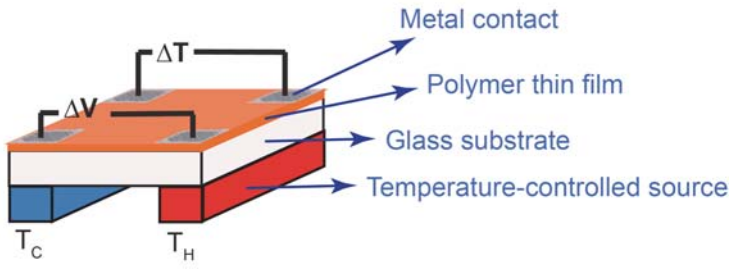

Figure 39. Schematic of the device used to measure the Seebeck coefficient of thin films.

6. CONCLUSIONS

Conjugated polymers contain a large density of delocalized electrons, thus, these polymers exhibit p-type behavior with n-type conjugated polymers being exceedingly rare. Unlike conjugated polymers, radical polymers undergo a reversible oxidation reduction reaction which enable radical polymers to have the potential to transport electrons just as well as holes. In this work, we focused on improving the transport properties of radical polymers while investigating the doping mechanism and altering the molecular architecture of the polymer. First, we have shown that dopants with sulfonic functional groups can improve the conductivity of a conjugated polymer and a radical polymer. Then, we introduced intramolecular dopants in PTMA through copolymerization. The copolymerization was synthesized by a free radical polymerization. Utilizing one batch of PTMPM-co-PVS, we oxidized for varying lengths of time to analyze how the oxidation affects carrier mobility and the functionality of the copolymer. We also measured the temperature dependence of the carrier mobility.

Ultimately, by understanding the molecular structure of a polymer and fine-tuning the functionality, the polymer's transport properties can be optimized. Through careful characterization and tailoring of new materials, organic material should proceed to a point where it is competitive with existing inorganic materials in the field of electrically conductive applications.

REFERENCES

REFERENCES

(1) H. Nishide, T. S. *Electrochem. Soc. Interface* 2005, 32–36.

(2) Guo, W.; Yin, Y. X.; Xin, S.; Guo, Y. G.; Wan, L. J. *Energy Environ. Sci.* 2012, *5*, 5221–5225.

(3) Janoschka, T.; Teichler, A.; Krieg, A.; Hager, M. D.; Schubert, U. S. *J. Polym. Sci. Part A Polym. Chem.* 2012, *50*, 1394–1407.

(4) Rostro, L.; Baradwaj, A. G.; Boudouris, B. W. *Appl. Mater. Interfaces* 2013, *5*, 9898–9901.

(5) Heeger, A. J. *J. Phys. Chem. B* 2001, *105*, 8475–8491.

(6) Heeger, A. J. *Chem. Soc. Rev.* 2010, *39*, 2354–2371.

(7) Shirakawa, H. *Synth. Met.* 2002, *125*, 3–10.

(8) Macdiarmid, A. G. *Synth. Met.* 2002, *125*, 11–22.

(9) Francioso, L.; De Pascali, C.; Farella, I.; Martucci, C.; Cretì, P.; Siciliano, P.; Perrone, a. *J. Power Sources* 2011, *196*, 3239–3243.

(10) Leonov, V.; Vullers, R. J. M. *J. Electron. Mater.* 2009, *38*, 1491–1498.

(11) Stark, I. In *Demonstration Paper : Integrating Thermoelectric Technology into Clothing for Generating Usable Energy to Power Wireless Devices*; Wireless Health: San Diego, 2012.

(12) Yazawa, K.; Shakouri, A. In *Energy Payback Optimization of Thermoelectric Power Generator Systems*; ASME: Vancouver, 2010; pp. 1–8.

(13) Ismail, B. I.; Ahmed, W. H. *Recent Patents Electr. Eng.* 2009, *2*, 27–39.

(14) Yazawa, K.; Shakouri, A. *Environ. Sci. Technol.* 2011, *45*, 7548–7553.

(15) Paul C. Hiemenz, T. P. L. *Polymer chemistry*; 2nd ed.; Taylor & Francis Group, LLC, 2007.

(16) Neil A. Dotson, Rafael Galvan, Robert L. Lawrence, M. T. *Polymerization process modeling*; John Wiley & Sons, Inc, 1996.

(17) Moad, G.; Chiefari, J.; Chong, B. Y. K.; Krstina, J.; Mayadunne, R. T. A.; Postma, A.; Rizzardo, E.; Thang, S. H. *Polym. Int.* 2000, *49*, 993–1001.

(18) Willcock, H.; O'Reilly, R. K. *Polym. Chem.* 2010, *1*, 149.

19) M. Fineman, S. R. *J. Polym. Sci.* 2011, *5*, 259–265.

(20) T. Kelen, F. Tudos, B. T. *Polym. Bull.* 1980, *2*, 71–76.

(21) Florjańczyk, Z.; Such, K.; Wieczorek, W. *J. Macromol. Sci. Part A* 1992, *29*, 853–863.

(22) Quinting, G. R.; Cai, R. *Macromolecules* 1994, *27*, 6301–6306.

(23) Ishitake, K.; Satoh, K.; Kamigaito, M.; Okamoto, Y. *Polym. Chem.* 2012, *3*, 1750–1757.

(24) Varshni, Y. P. *J. Phys. Chem. Solids* 1979, *40*, 791–793.

(25) Moraga, L. A. *J. Phys. Condens. Matter* 1990, *2*, 3777–3795.

(26) Sakanoue, T.; Sirringhaus, H. *Nat. Mater.* 2010, *9*, 736–740.

(27) Bozano, L.; Carter, S. a.; Scott, J. C.; Malliaras, G. G.; Brock, P. J. *Appl. Phys. Lett.* 1999, *74*, 1132–1134.

(28) Giulianini, M.; Waclawik, E. R.; Bell, J. M.; Motta, N. *J. Appl. Phys.* 2010, *108*, 014512–1 – 014512–014514.

(29) Kaake, L. G.; Barbara, P. F.; Zhu, X.-Y. *J. Phys. Chem. Lett.* 2010, *1*, 628–635.

(30) S. Sze, K. N. *Physics of Semiconductor Devices*; 3rd ed.; John Wiley & Sons, Inc, 2007.

(31) Wang, L.; Akimov, A. V; Chen, L.; Prezhdo, O. V. *J. Chem. Phys.* 2013, *139*, 174109–1– 174109–174110.

(32) Zhu, W.; Perebeinos, V.; Freitag, M.; Avouris, P. *Phys. Rev. B* 2009, *80*, 235402–1– 235402–235408.

(33) Kalb, W. L.; Haas, S.; Krellner, C.; Mathis, T.; Batlogg, B. *Phys. Rev. B* 2010, *81*, 155315–1– 155315–13.

(34) Janoschka, T.; Hager, M. D.; Schubert, U. S. *Adv. Mater.* 2012, *24*, 6397–6409.

(35) Luo, X.; Mather, P. T. *ACS Macro Lett.* 2013, *2*, 152–156.

(36) Shakouri, A.; Li, S.; Cruz, S. In *Thermoelectric Power Factor for Electrically Conductive Polymers*; 18th International Conference on Thermoelectrics, 1999; pp. 402–406.

(37) Shakouri, A. *Annu. Rev. Mater. Res.* 2011, *41*, 399–431.

(38) Inc, B. In *Waste Heat Recovery: Technology Opportunities in the US Industry*; US Department of Energy, 2008; pp. 1–112.

(39) Snyder, G. J.; Toberer, E. S. *Nat. Mater.* 2008, *7*, 105–114.

(40) Rowe, D. M. *CRC handbook of thermoelectrics*; CRC Press: Boca Raton, 1995.

(41) Kraemer, D.; Poudel, B.; Feng, H.-P.; Caylor, J. C.; Yu, B.; Yan, X.; Ma, Y.; Wang, X.; Wang, D.; Muto, A.; McEnaney, K.; Chiesa, M.; Ren, Z.; Chen, G. *Nat. Mater.* 2011, *10*, 532–538.

(42) Poehler, T. O.; Katz, H. E. *Energy Environ. Sci.* 2012, *5*, 8110–8115.

(43) Cahill, D. G. *Phys. Rev. B* 1992, *46*, 6131–6140.

(44) Nielsen, M. D.; Ozolins, V.; Heremans, J. P. *Energy Environ. Sci.* 2013, *6*, 570–578.

(45) Kim, W.; Zide, J.; Gossard, A.; Klenov, D.; Stemmer, S.; Shakouri, A.; Majumdar, A. *Phys. Rev. Lett.* 2006, *96*, 045901–1– 045901–045904.

(46) E. Steigmeier, B. A. *Phys. Rev.* 1964, *136*, A1149–A1155.

(47) Ma, L.; Lee, W. H.; Park, Y. D.; Kim, J. S.; Lee, H. S.; Cho, K. *Appl. Phys. Lett.* 2008, *92*, 063310–063311– 063310–063313.

(48) Liu, C.-Y.; Chen, S.-A. *J. Phemical Phys.* 2009, *130*, 204906–1– 204906–6.

(49) Nam, S.; Shin, M.; Park, S.; Lee, S.; Kim, H.; Kim, Y. *Phys. Chem. Chem. Phys.* 2012, *14*, 15046–15053.

(50) Shen, X.; Duzhko, V. V.; Russell, T. P. *Adv. Energy Mater.* 2013, *3*, 263–270.

(51) Yue, R.; Xu, J. *Synth. Met.* 2012, *162*, 912–917.

(52) Kim, K. T.; Kim, K. J.; Ha, G. H. *Electron. Mater. Lett.* 2010, *6*, 177–180.

(53) See, K. C.; Feser, J. P.; Chen, C. E.; Majumdar, A.; Urban, J. J.; Segalman, R. a. *Nano Lett.* 2010, *10*, 4664–4667.

(54) Park, Y. W. *Synth. Met.* 1991, *45*, 173–182.

(55) Kim, G.-H.; Shao, L.; Zhang, K.; Pipe, K. P. *Nat. Mater.* 2013, *12*, 719–723.

(56) Bubnova, O.; Khan, Z. U.; Malti, A.; Braun, S.; Fahlman, M.; Berggren, M.; Crispin, X. *Nat. Mater.* 2011, *10*, 429–433.

(57) He, M.; Qiu, F.; Lin, Z. *Energy Environ. Sci.* 2013, *6*, 1352–1361.

(58) Zhang, Y.; Basel, T. P.; Gautam, B. R.; Yang, X.; Mascaro, D. J.; Liu, F.; Vardeny, Z. V. *Nat. Commun.* 2012, *3*, 1–7.

(59) Bauer, U.; Emori, S.; Beach, G. S. D. *Nat. Nanotechnol.* 2013, *8*, 411–416.

(60) Tsarevsky, N. V.; Braunecker, W. a.; Tang, W.; Brooks, S. J.; Matyjaszewski, K.; Weisman, G. R.; Wong, E. H. *J. Mol. Catal. A Chem.* 2006, *257*, 132–140.

(61) McLachlan, F.; Mathews, C. J.; Smith, P. J.; Welton, T. *Organometallics* 2003, *22*, 5350–5357.

(62) Nikiforov, M. P.; Lai, B.; Chen, W.; Chen, S.; Schaller, R. D.; Strzalka, J.; Maser, J.; Darling, S. B. *Energy Environ. Sci.* 2013, *6*, 1513–1520.

(63) Krebs, F. C.; Nyberg, B.; Jørgensen, M.; Energy, A. B. S.; Sol, M. *Chem. Mater.* 2004, *16*, 1313–1318.

(64) Nakahara, K.; Iwasa, S.; Satoh, M.; Morioka, Y.; Iriyama, J.; Suguro, M.; Hasegawa, E. *Chem. Phys. Lett.* 2002, *359*, 351–354.

(65) Suga, T.; Pu, Y.; Kasatori, S.; Nishide, H. *Macromolecules* 2007, *40*, 3167–3173.

(66) Oyaizu, K.; Nishide, H. *Adv. Mater.* 2009, *21*, 2339–2344.

(67) Bugnon, L.; Morton, C. J. H.; Novak, P.; Vetter, J.; Nesvadba, P. *Chem. Mater.* 2007, *19*, 2910–2914.

(68) Yonekuta, Y.; Susuki, K.; Oyaizu, K.; Honda, K.; Nishide, H. *J. Am. Chem. Soc.* 2007, *129*, 14128–14129.

(69) Kemper, T.; Larsen, R. E.; Gennett, T. *J. Phys. Chem. C* 2014, (submitted).

(70) Okayasu, T.; Hibino, T.; Nishide, H. *Macromol. Chem. Phys.* 2011, *212*, 1072–1079.

(71) Nam, S.; Kim, J.; Lee, H.; Kim, H.; Ha, C.-S.; Kim, Y. *ACS Appl. Mater. Interfaces* 2012, *4*, 1281–1288.

(72) Deore, M. F. *Self-doped Conducting Polymers*; John Wiley & Sons, Inc: England, 2007.

(73) López-Peña, H. a; Hernández-Muñoz, L. S.; Frontana-Uribe, B. a; González, F. J.; González, I.; Frontana, C.; Cardoso, J. *J. Phys. Chem. B* 2012, *116*, 5542–5550.

(74) Smith, L. M.; Coote, M. L. *J. Polym. Sci. Part A Polym. Chem.* 2013, *51*, 3351–3358.

(75) Zhenkun Ma, J. M. B. *J. Org. Chem* 1991, *56*, 6110–6114.

(76) Pinal, R. *Entropy* 2008, *10*, 207–223.

(77) Schneider, H. A. *Makromol. Chem.* 1988, *189*, 1941–1955.

(78) Chae, I. S.; Koyano, M.; Oyaizu, K.; Nishide, H. *J. Mater. Chem. A* 2013, *1*, 1326–1333.

(79) Rostro, L.; Wong, S. H.; Boudouris, B. W. *Macromolecules* 2014, *47*, 3713–3719.

(80) Grampp, G.; Landgraf, S.; Rasmussen, K.; Strauss, S. *Spectrochim. Acta Part A* 2002, *58*, 1219–1226.

(81) Carbone, a.; Kotowska, B.; Kotowski, D. *Phys. Rev. Lett.* 2005, *95*, 236601–1–236601–236604.

(82) Koehler, M.; Biaggio, I. *Phys. Rev. B* 2004, *70*, 045314–1– 045314–045318.

(83) Lim, S. H. N.; McKenzie, D. R.; Bilek, M. M. M. *Rev. Sci. Instrum.* 2009, *80*, 075109–1– 075109–4.

(84) De Boor, J.; Schmidt, V. *Adv. Mater.* 2010, *22*, 4303–4307.